J Math Chem (2009) 45:819–858
DOI 10.1007/s10910-008-9484-2

ORIGINAL PAPER

Unequivocal resolution of multiplets in MR spectra for prostate cancer diagnostics achieved by the fast Padé transform

Dževad Belkić · Karen Belkić

Received: 1 September 2008 / Accepted: 6 October 2008 / Published online: 4 November 2008

Abstract We perform mathematical modeling with the fast Padé transform (FPT) according to magnetic resonance (MR)-time signals as encoded in vitro from normal glandular and stromal prostate tissue and from prostate cancer. This is one of the most demanding signal processing problems in MR spectroscopy due to the abundance of diagnostically important multiplets (notably doublet and triplet resonances). The FPT provided exact reconstruction at short acquisition times (i.e. using only a fraction of the full signal length) of all the input spectral parameters for the data corresponding to prostate cancer and to normal glandular as well as stromal prostate tissue. This was achieved without any fitting or numerical integration of peak areas. The converged parametric results remained stable at longer partial signal lengths, including the case using the full signal length. The Padé absorption component spectra yielded unequivocal resolution of all the extracted physical resonances, including multiplet resonances and closely overlapping peaks of different metabolites. The capacity of the FPT to resolve and precisely quantify the physical resonances as encountered in normal tissue from two distinct regions of the prostate, as well as in prostate cancer is demonstrated. The spectra from prostate tissues are dense, which suggests that there is a rich array of metabolic information to be gleaned. The FPT is hereby shown to be optimally suited to retrieve that information. The FPT reliably yields the metabolite concentrations

D. Belkić (✉) · K. Belkić
Department of Oncology/Pathology, Karolinska Institute, P.O. Box 260, Stockholm 17176, Sweden
e-mail: Dzevad.Belkic@ki.se

K. Belkić
Institute for Prevention Research, University of Southern California Keck School of Medicine, Los Angeles, CA 91803, USA
e-mail: Karen.Belkic@ki.se

that could be of critical importance for distinguishing non-malignant from cancerous prostate tissue. Padé-optimized MRS could clearly aid prostate cancer diagnostics. This line of investigation will continue with experimentally encoded data from normal, hypertrophic and cancerous prostate tissue, in vitro and in vivo. We anticipate that Padé-optimized MRS will improve the specificity as well as sensitivity of MR-based modalities with respect to prostate cancer. This could have an important impact upon timely and accurate diagnosis of this malignancy, as well as aiding decision-making for therapeutic dilemmas.

Keywords Prostate cancer · Benign prostatic hypertrophy · Magnetic resonance spectroscopy · Time signals · Quantification · Fast Padé transform

Abbreviations

Ala	Alanine
au	Arbitrary units
Cit	Citrate
Cho	Choline
Cr	Creatine
DRE	Digital rectal examination
FID	Free induction decay
FFT	Fast Fourier transform
FPT	Fast Padé transform
FWHM	Full width at half maximum
GPC	Glycerophosphocholine
HLSVD	Hankel-Lanczos Singular Value Decomposition
HRMAS	High-resolution magic-angle spinning
Lac	Lactate
m-Ino	Myoinositol
MR	Magnetic resonance
MRI	Magnetic resonance imaging
MRS	Magnetic resonance spectroscopy
MRSI	Magnetic resonance spectroscopic imaging
PA	Polyamines
PC	Phosphocholine
ppm	Parts per million
PSA	Prostate specific antigen
s-Ino	Scyllo-inositol
SNR	Signal-to-noise ratio
SNS	Signal-noise separation
Tau	Taurine
TE	Echo time
TRUS	Transurethral ultrasound
TSP	3-(Trimethylsilyl-) 3,3,2,2-tetradeutero-propionic acid

1 Introduction

Carcinoma of the prostate is the most frequently diagnosed visceral cancer, and the most common cancer among men [1,2]. The number of detected cases of prostate cancer has increased dramatically in the 1990s based on the widespread testing with prostate specific antigen (PSA) [3]. Notwithstanding the potential benefits it provides for early detection of prostate cancer, screening with PSA has also lead to many diagnostic and therapeutic dilemmas, for which magnetic resonance imaging (MRI) and spectroscopic imaging (MRSI) have become of critical importance. Unfortunately, however, insufficient accuracy of all the customary data processing algorithms that are built into clinical scanners has been a major impediment to progress, especially for diagnostic modalities based upon magnetic resonance spectroscopy (MRS) and MRSI.

The most commonly used analytical technique in MRS is the fast Fourier transform (FFT). Although computationally stable, the FFT only estimates the total shape of the spectrum, and does so with low-resolution, which is equal to $2\pi/T$ where T is the total acquisition time. Within the FFT, a complex-valued Fourier spectrum is defined by using only *a single polynomial*:

$$F = \frac{1}{N}\sum_{n=0}^{N-1} c_n e^{2i\pi nk/N}; \quad 1 \le k \le N-1. \tag{1}$$

The FFT is a linear transform, and, as such, imports noise as intact from the time to the frequency domain, further contributing to poor signal to noise ratio (SNR) [4]. Furthermore, FFT lacks extrapolation capacities based upon the analyzed time signal, or equivalently, the free induction decay (FID).

The FFT is limited to non-parametric estimation, and thus provides only the total shape of spectral structures, but does not specify the number of components nor does it provide quantification. Peak parameters are subsequently extracted in post-processing by fitting, but this is not unique. Thus, for example, 2, 3 or more resonances can yield the same fit for the overall shape of a given structure, and there is no way to be certain which of the fits is correct. These problems are most pronounced for overlapping resonances, which are often clinically important [5]. Besides the fact that fitting is non-unique, much information contained in the signal is not obtained in an adequate way, such that estimates for position, width, height and phase of resonances can be biased [4]. Metabolite concentrations can only be accurately computed if these parameters are obtained in a reliable way with an intrinsic and robust error analysis [4].

Much more information could be provided from MRS and MRSI insofar as the optimally suited data analysis were performed [6]. This paper will examine the potential advantages of a more advanced mathematical approach to processing MRS time signals through the fast Padé transform (FPT), and how this could specifically impact upon problem areas within prostate cancer diagnostics and therapeutics. Prostate-related time signals pose a special challenge to spectral analysis. This is due to the appearance of dense spectra packed tightly with multiplets such as doublet and triplet resonances.

1.1 Brief theoretical background of the fast Padé transform for processing MRS time signals and relevance for cancer diagnostics

We have performed "*proof of principle*" investigations [4,7–16] which clearly show that FPT is a powerful and stable signal processor, which provides robust error analysis and quantifies MRS time signals unequivocally.

The FPT is a non-linear *polynomial quotient* P_L/Q_K of the exact finite-rank spectrum (Green function) given by the Maclaurin series with the encoded raw time signal $\{c_n\}$ as the expansion coefficients. The FPT, as the ratio of two polynomials represents the optimal mathematical model for the frequency spectrum. This is prescribed quantum-mechanically. The same physics in the form of the time signal as the sum of complex-valued damped exponentials, by virtue to the time-frequency dual representation, automatically prescribes that the frequency spectrum is given by the Padé quotient of two polynomials. Thus, there is a fundamental theoretical basis for the proven algorithmic success of the FPT [4,11,14].

The non-linearity of the FPT facilitates noise suppression. Unlike many other parametric estimators, the FPT is stable when signal length is systematically increased at a fixed bandwidth and it does not generate spikes or other spectral deformations [4,17]. The FPT is a powerful interpolator and extrapolator [4]. Due to extrapolation, which is present in the implicit polynomial inversion via Q_K^{-1} in P_L/Q_K, inference is gained from a non-measurable infinite number of signal points by using only the available finite set $\{c_n\}(0 \leq n \leq N-1, N < \infty)$. While the FPT can use the fixed Fourier mesh $2\pi k/T(k = 0, \ldots, N-1)$, this is not obligatory. In other words, the FPT can be computed at any frequency ω. Resolution in the FPT is not pre-determined by T. Due to its parametric estimation, as well as interpolation and extrapolation capabilities, the FPT has better resolving power than the FFT.

By using the concept of Froissart doublets (pole-zero cancellations) [18], the FPT can unequivocally identify and separate noise from the genuine/physical content of the signal [13–16]. The FPT thereby provides complete separation of noise from the genuine metabolic information even in the presence of random Gauss-distributed zero mean noise at the level typically encountered in clinically encoded MR-time signals [16]. For noiseless MRS time signals, the FPT returns all the spectral parameters (irrespective of their number) within machine accuracy [14,15,19]. Moreover, our algorithm from Refs. [13,14,19] demonstrates an unprecedented robustness, even against round-off-errors, since e.g. 12-digit accurate input parameters can be reconstructed with all the 12 digits exactly. For noise-corrupted FIDs, all the known physical/genuine spectral parameters are retrieved by the FPT within at least 3–4 decimal places for SNR of those typically encountered in time signals encoded via MRS [14,16]. It should be emphasized, in addition, that the number of spurious resonances is always greater than that of the true resonances.

The polynomial quotient P_K/Q_K (diagonal) or P_{K-1}/Q_K (para-diagonal) as a rational function in harmonic variable $z^{-1} = \exp(-i\omega\tau)$, is known in the literature as the Padé approximant [20,21]. In signal processing, the Padé approximant is alternatively called the fast Padé transform [20,21] to emphasize the possibility of obtaining a shape spectrum from an FID via a non-parametric estimation as reminiscent of the FFT. The latter type of estimation in the FPT is done by simply evaluating the Padé

spectrum P_K/Q_K without ever searching for any of the spectral parameters that are the complex frequencies $\{\omega_k\}$ and amplitudes $\{d_k\}$. The FPT is the only parametric estimator which computes the envelope spectrum without the need to obtain the set $\{\omega_k, d_k\}$ first. This is in sharp contrast to e.g. Hankel-Lanczos Singular Value Decomposition (HLSVD) [22] which computes the envelope spectrum by first estimating the peak parameters $\{\omega_k, d_k\}$.

Most importantly, the FPT provides parametric reconstructions by rooting the polynomial Q_K whose roots $\{z_k^{-1}\}$ yield the fundamental frequencies $\{\omega_k\}$ and this leads to the corresponding amplitudes $\{d_k\}$ for each resonance. A time signal which yields a Lorentzian (non-degenerate) spectrum as the sum of K exponentials with constant amplitudes $\{d_k\}(1 \le k \le K)$, is given by:

$$c(t) = \sum_{k=1}^{K} d_k e^{-i\omega_k t}. \tag{2}$$

For example, the para-diagonal FPT treats the exact spectrum, i.e. the mentioned finite-rank Green function $G_N(z^{-1})$, via the *unique* ratio of two polynomials $P_{K-1}(z^{-1})/Q_K(z^{-1})$ at *any frequency* ω:

$$G_N(z^{-1}) = \frac{1}{N}\sum_{n=0}^{N-1} c_n z^{-n}, \tag{3}$$

$$G_N(z^{-1}) \approx \frac{P_{K-1}(z^{-1})}{Q_K(z^{-1})} = \sum_{k=1}^{K} \frac{d_k}{z^{-1} - z_k^{-1}}, \tag{4}$$

$$P_{K-1}(z^{-1}) = \sum_{r=0}^{K-1} p_r z^{-r}, \quad Q_K(z^{-1}) = \sum_{s=0}^{K} q_s z^{-s}, \tag{5}$$

where $z = e^{i\omega\tau}$ and $z_k = e^{i\omega_k\tau}$. The para-diagonal ($L = K - 1$) and diagonal ($L = K$) FPT are most frequently used from the set of the general polynomial quotients of the type, P_L/Q_K, because they are the most stable and incur minimal error in practice. In the FPT, the sum $\sum_{k=1}^{K} d_k/(z^{-1} - z_k^{-1})$ represents the complex-valued *total shape spectrum* (envelope) which is the linear combination of the K corresponding *component spectra*, $d_k/(z^{-1} - z_k^{-1})(1 \le k \le K)$. Here, P_{K-1} and Q_K are readily extracted from the input data G_N by treating the product $G_N Q_K$ in the defining relation $G_N * Q_K = P_{K-1}$ as the standard convolution [4,7,20].

The above formulae are valid for non-degenerate spectra, i.e. for all distinct roots $\{z_k^{-1}\}$. When some of the z_k's coincide with each other (degenerate roots—leading to overlapping resonances), the above formulae should be modified. In that case, the c_n's corresponding to the *physical* non-Lorentzian spectrum with degenerate (multiple) roots $\{z_k\}$ read as:

$$c_n = \sum_{k=1}^{J}\sum_{m_k=1}^{M_k} d_{k,m_k}(n\tau)^{m_k-1} e^{-in\tau\omega_k}, \quad \mathrm{Im}(\omega_k) < 0. \tag{6}$$

Hereafter, Re(z) and Im(z) denote, respectively, the real and imaginary parts of the complex number z. If the kth root z_k of $Q_K(z)$ has $M_k \leq K$ multiplicity, then the Padé spectrum is modified via:

$$\frac{P_{K-1}(z)}{Q_K(z)} = \sum_{k=1}^{J} \sum_{m_k=1}^{M_k} \frac{d_{k,m_k}}{(z - z_k)^{m_k}}, \tag{7}$$

where $M_1 + M_2 + \cdots + M_J = K$. Here d_{k,m_k} are the new amplitudes given as:

$$d_{k,m_k} = \frac{P_{K-1}(z_k)}{Q_K^{(m_k)}(z_k)}, \tag{8}$$

where $Q_K^{(m)}(z)$ is the mth derivative of the denominator polynomial $Q_K(z)$,

$$Q_K^{(m)}(z) = \frac{d^m}{dz^m} Q_K(z). \tag{9}$$

However, also for the degenerate roots of the characteristic or secular equation, $Q_K(z) = 0$, for the given N values of the c_n's, one always obtains the unique quotient P_{K-1}/Q_K. A Lorentzian model is applied for quantification of spectra with clearly separated/isolated resonances. A non-Lorentzian model is used for quantifying spectra with overlapping resonances. This ability of the FPT to handle degenerate spectra is advantageous, particularly compared to other parametric methods such as HLSVD or Linear Predictor, which are limited to Lorentzian models. Since MR spectra are abundant with overlapping resonances, the ability to treat non-Lorentzian and Lorentzian spectra on the same footing provides yet another reason why the FPT is optimally suited for processing MRS data [4].

These findings have been assessed in direct relation to clinical oncology. In addition to demonstrating the high resolution and stability of the FPT in general studies of MR total shape spectra, a superior overall performance of the FPT has also been clearly shown for data directly relevant to oncology. These include cancerous and non-cancerous samples from the ovary [23,24] and from the breast [25]. The FPT markedly enhanced the resolution of the MR spectra compared to the conventional Fourier analysis, but it also yielded the exact parametric data needed to reconstruct the metabolite concentrations which characterize ovarian and breast cancer and distinguish this from non-malignant lesions. Moreover, complete separation of noise from the genuine metabolic information, i.e. signal-noise separation (SNS) has been achieved via pole-zero cancellations with the FPT for spectrally dense regions that were seen within data derived from the breast, in which there were over 100 times more spurious compared to genuine resonances. The Padé absorption spectra yielded the highest resolution of all the extracted physical resonances, even of those that were nearly degenerate, and thereby unambiguously delineated and quantified diagnostically important metabolites that may represent MR-retrievable molecular markers of breast cancer [25].

1.2 Prostate cancer diagnostics: present status and the role of MRS and MRSI

Since the mid 1990s the mortality rate from prostate cancer has been decreasing. Early detection and active treatment are considered to have been the main reasons for this favorable trend [2]. Screening with PSA is likely to have contributed to this positive development. However, no cutpoints have been identified that yield both optimal sensitivity and specificity [26]. This widespread screening has led to an increased detection of localized tumors, decreased frequency of nodal spread and of late stage detection, all of which improve survival dramatically. Notwithstanding the lack of randomized controlled evidence to support their recommendation, screening with PSA plus digital rectal examination (DRE) is recommended by the American Cancer Society and the American Urological Association, though not by the American College of Preventive Medicine [27]. However, it must also be noted that over-detection and over-treatment can be harmful [3]. The negative potential consequences of screening include patient discomfort from prostate biopsy and psychological effects of a false-positive result. Moreover, treatment has a number of important side-effects. Thus, most recently, the U.S. Preventive Services Task Force have recommended *against* screening for prostate cancer among men aged 75 years or older [28]. A recent meta-analysis concerning the benefits and harms of screening with PSA found that there is (a) a lack of good-quality randomized, controlled studies, (b) cross-sectional and longitudinal evidence of deleterious psychological effects of a false-positive PSA screening result, and (c) the benefit of screening with PSA is uncertain [29].

The standard practice is that when prostate cancer is suspected on the basis of abnormal PSA and/or DRE, prostate biopsy guided by transurethral ultrasound (TRUS) is usually recommended. However, TRUS has limited sensitivity for visualizing prostate cancers, and thus at least 8, and according to some authors 12 cores should be obtained [1,2]. Even with this large number of samples, TRUS-guided biopsy has a sensitivity of about 80%, which means that approximate 20% of prostate cancers remain undetected [1,3]. On the other hand, since PSA has low specificity (high false positive rates) —up to 75% of patients who are biopsied for elevated PSA do not actually have prostate cancer [30].

In the recent period, striking attention has been paid in leading investigative clinical journals to in vivo MRS and MRSI as a potentially key non-invasive modality for prostate cancer diagnostics [31–35]. Spectroscopic imaging through in vivo magnetic resonance has made a major impact in prostate cancer, where this method provides diagnostic clarity unmatched by literally any other non-invasive approach. Compared to MRI alone, MRSI substantially improves the accuracy with which prostatic tumor and extracapsular extension are detected, as well as helping to distinguish cancerous prostate from benign prostatic hypertrophy [36]. Guidance as to the optimal site for biopsy has been substantially improved by MRSI. Other areas of clinical decision-making with respect to prostate cancer have been impacted as well by MRSI. These include e.g. selection of treatment modality and timing, treatment planning with brachytherapy, and assessing tumor regression versus recurrence after treatment.

The ratio between two magnetic resonance observable metabolites, choline at $\sim$3.2 ppm (parts per million, the unit for dimensionless frequencies) and citrate ($\sim$ 2.5–2.7 ppm), has been the cornerstone of applications of in vivo MRSI for

prostate cancer detection. Citrate is generally used as an indicator of healthy secretory activity of prostate epithelial cells, while choline reflects phospholipid metabolism of cell membranes, and is a marker for membrane damage, cellular proliferation and density typical of malignant processes.

There are, however, clinically important exceptions with respect to these two metabolites. For example, in stromal prostate tissue or metabolic atrophy, citrate levels are low without cancer being present. With hypertrophic prostate, citrate can still be high despite coexistent malignancy. Overall, it has been noted that citrate and choline alone are not sufficiently accurate markers for distinguishing between various patterns of prostatic disease [37]. Furthermore, normal citrate concentrations vary between the central gland and peripheral zone, and this must also be taken into account when interpreting choline-to-citrate ratios. In general, metabolite ratios are problematic, being dependent upon echo time (TE) [38] and affected by confounding factors including cancer treatment itself [37]. Moreover, MRS and MRSI for prostate cancer are reported to have generally rather limited sensitivity in the analysis of smaller lesions, and this is the usual way that this type of cancer typically first presents [39]. Kundra and colleagues [2] have cited limitations in the resolution and interpretation of data from MRSI as important challenges with respect to prostate cancer diagnosis, staging and surveillance.

In vitro MRS reveals other metabolites whose levels help identify prostate cancer; these include: spermine, spermidine, polyamines, lysine, myoinositol, scyllo-inositol and taurine, *inter alia* [40]. The first three of these are assigned to 3.1 ppm and lie therefore very close to choline at 3.2 ppm. Myoinositol has a short T_2 relaxation time and, therefore, will have decayed at longer TE. In marked contrast to the usual basis for diagnosing prostate cancer by in vivo MRS, Swindle et al. [40] found in their study of 77 prostate specimens from the prostate, "depleted citrate and elevated choline levels alone were not accurate markers of malignancy, since citrate levels remain high when a small amount of malignant disease is present" (p. 144). On the other hand, they found that lipid, creatine and lysine were helpful.

Using high-resolution magic-angle spinning (HRMAS), Swanson et al. [41] assessed 54 post-surgical prostate samples obtained using 3-dimensional MRSI. Healthy glandular tissue was distinguished from prostate cancer by significantly higher levels of citrate and polyamines, and lower choline, phosphocholine and glycerophosphocholine. Predominantly stromal tissue lacked citrate and polyamines, but had significantly lower levels of choline compounds compared to malignant tissue. Taurine, myoinositol and scyllo-inositol as well as choline compounds were higher in prostate cancer. More aggressive cancers showed higher choline and lower citrate and polyamines. The authors conclude: "the elucidation of spectral patterns associated with mixtures of different prostate tissue types and cancer grades, and the inclusion of new metabolic markers for prostate cancer may significantly improve the clinical interpretation of in vivo prostate MRSI data" (p. 944). More recently, Swanson et al. [42] reported metabolite concentrations from 60 post-surgical samples of healthy glandular and stromal prostate tissue as well as for prostate cancer using HRMAS. The malignant prostate samples were significantly distinguished from both these normal tissues by higher concentrations of lactate (1.34 and 4.14 ppm), phosphocholine (3.23 ppm) plus glycerophosphocholine (3.24 ppm) and total choline. Only in comparison to healthy

glandular tissue did prostate cancer differ significantly with respect to lower citrate (2.54 and 2.72 ppm) and polyamines (3.10 and 3.14 ppm). On the other hand, the prostate cancer specimens had significantly higher concentrations of alanine (1.49, 2.54, 2.72 ppm) and choline (3.21 ppm) than the healthy stromal tissue, but these concentrations differed only at a borderline level of significance for healthy glandular tissue versus prostate cancers. Swanson et al. [42] noted that spectral overlap was a major problem in 1D HRMAS studies of prostate cancer and other tissues. A particular challenge for quantification in Ref. [42] was the resolution of the abundant multiplet resonances in the spectra of prostate.

In the present study we examine the performance of the FPT applied to theoretically generated time signals that are reminiscent of in vitro MRS data as encoded from extracted prostate specimens from Ref. [42]. This is viewed as the first step in the process of determining whether the described features of the FPT could be of potential benefit for prostate cancer diagnostics via MRS, with a special view to the resolution and quantification of multiplet resonances and closely overlapping resonances of different metabolites.

2 Results

2.1 Input data

2.1.1 Recapitulation of the findings from Ref. [42]

The FIDs from Ref. [42] were recorded at a Larmor frequency of 500 MHz corresponding to a static magnetic field strength of B_0 = 11.7 T. In Ref. [42] the mean concentrations (expressed in mM/kg = μM/g) were given for healthy glandular and stromal prostate tissue, as well as for prostate cancer derived from 60 post-surgical samples and prostate cancer. In Ref. [42] each FID was apodized using a 0.5 Hz matched exponential filter, zero-filled to 65536 complex points and Fourier transformed. The baseline of the entire spectrum was fitted using a sixth-order polynomial function, which was then subtracted from the spectrum. Metabolites were quantified by Lorentzian-Gaussian peak fitting using the Levenberg-Marquardt algorithm. The goodness of fit was assessed by comparing the difference between the total shape spectra and the fitted peaks, and this was considered satisfactory when this difference (residual) was minimal.

There was a total of 10 mean metabolite concentrations cited in Ref. [42] respectively for healthy glandular and stromal prostate tissue and for prostate cancer. Only four of these metabolites concentrations were calculated on the basis of a single peak: alanine (Ala) at 1.49 ppm, creatine (Cr) at 3.04 ppm, free choline (Cho) at 3.21 ppm and scyllo-inositol (s-ino) at 3.35 ppm. The remaining metabolite concentrations were based upon multiplet resonances that were all fitted, as follows: Citrate (Cit) was fitted to a doublet of doublets at 2.54 and 2.72 ppm. The taurine (Tau) concentrations were based upon two triplets, one centered at 3.26 ppm and the other at 3.43 ppm. The myoinositol (m-Ino) concentration was calculated from two triplets centered at 3.55 and 3.64 ppm plus a singlet at 4.07 ppm. The lactate concentration was based upon a very large peak at 1.33 ppm and a smaller one at 4.12 ppm. The sum of singlet

phosphocholine (PC) at 3.23 ppm and glycerophosphocholine (GPC) at 3.24 ppm was also given, but not the individual components. Polyamine (PA) concentrations were based upon the spermine concentrations from two broad single peaks at 3.10 and 3.14 ppm.

2.1.2 Challenges with spectral crowding from Ref. [42]: Multiplets and overlapping resonances of different metabolites

As mentioned, Swanson et al. [42] reported that spectral overlap was a major problem in 1D HRMAS studies of prostate cancer and other tissues. They noted, for example, that phosphocholine at 3.23 ppm and glycerophosphocholine at 3.24 ppm could not be resolved from each other; and the sum of these two metabolites concentration was therefore given.

Moreover, within the spectra, the numerous multiplets represented a particular challenge. All of these multiplets were based upon fitting which is not unique. Within the regions of greatest spectral density, the difficulties become even greater. Of the polyamine resonances, only the contribution from the predominant spermine was included, whereas putrescine and spermidine could not be resolved.

These challenges underscore the need for exact, unequivocal quantification not only of non-degenerate spectra with distinct roots, but also for multiplets with overlapping resonances. The FPT would appear to be ideally suited to this task.

2.1.3 Input data for the present analysis

We synthesized three FIDs of the type:

$$c_n = \sum_{k=1}^{K} d_k e^{in\omega_k \tau}, \quad \mathrm{Im}(\omega_k) > 0. \tag{10}$$

via a sum of $K = 27$ damped complex exponentials $\exp(in\tau\omega_k)(1 \leq k \leq 27)$ with time-independent (stationary) complex amplitudes d_k. Here, ω_k and d_k are the fundamental angular frequencies and amplitudes ($\omega_k = 2\pi f_k$, with f_k being the linear frequency). These time signals were subsequently quantified using the FPT, as described in Ref. [13]. We used a bandwidth of 6000 Hz (the inverse of this bandwidth is the sampling time τ) and set the total signal length $N = 1024$.

The input data were built according to the given mean metabolite concentrations, description of multiplets and the total shape spectra for the normal glandular prostate, normal stromal prostate and prostate cancer from Ref. [42]. Thus, the total metabolite concentrations were split into multiplets to proportionally match the spectra of Ref. [42] and to fill in lacunae.

We computed the input peak amplitudes d_k from the reported metabolite concentrations C_k, where $|d_k| = (C_k/C_{ref}) \times 2$. The reference material was TSP (3-(trimethylsilyl-) 3,3,2,2-tetradeutero-propionic acid). The concentration of TSP, C_{ref} was calculated as follows from the data reported in Ref. [42]. Therein, there was a total of (TSP + D_20) = 3.79 mg, where TSP comprised 0.75% of that weight. Thus, there

were 0.02845 mg of TSP. Since the molecular weight of TSP = 172.23 g, there were 0.1652 μM of TSP and the mass of wet tissue = 15.11 mg, such that the concentration of TSP = 0.1652 μM/15.11 mg = 10.93 μM/g.

The phases $\varphi_k (1 \leq k \leq 27)$ from complex-valued d_k were all set to zero, so that every d_k becomes real, $d_k = |d_k|$.

The input data are given for the normal glandular, stromal prostate and for prostate cancer in Tables 1–3, respectively.

2.2 Reconstruction of the data using the FPT

We used the diagonal FPT to analyze the FIDs. The coefficients $\{p_r, q_s\}$ of the polynomials P_K and Q_K were computed by solving the systems of linear equations, treating the product in $G_N(z^{-1}) * Q_K(z^{-1}) = P_K(z^{-1})$ as a convolution. To extract the peak parameters, we solved the characteristic equation $Q_K(z^{-1}) = 0$. This leads to K unique roots $z_k^{-1} (1 \leq k \leq K)$, so that the sought ω_k is deduced via $\omega_k = (i/\tau) ln(z_k^{-1})$. The FPT extracts the parameters $\{\omega_k, d_k\} (1 \leq k \leq K)$ of every physical resonance directly from the raw encoded FID. The kth metabolite concentration is computed from the reconstructed amplitudes d_k as $C_{met}(|d_k| \times C_{ref})/2 = 5.465 \times |d_k|$(μM/g) of the tissue wet weight.

To establish the constancy of the spectral parameters for all three signals, we systematically increased the signal length for the same bandwidth. Examining the spectral parameters at total orders $K = 250$, 300 and 350 where $2K = N_P$ and N_P denotes partial signal length, we found that convergence occurred at $K = 350$, 300 and 300 for all the FIDs in the respective cases of normal glandular and normal stromal prostate and for prostate cancer. These all remained stable thereafter. We determined whether a given reconstructed resonance was true or spurious by computing a sequence of the Padé shape spectra $\{P_m/Q_m\} (m = 1, 2, 3, \ldots)$ in the whole Nyquist range, which includes the frequency range of interest from 1.3 to 4.2 ppm, as described in Ref. [14]. For the first examined FIDs, of the 350 total resonances, 323 were identified as spurious by their zero amplitudes and the pole-zero coincidences, yielding the 27 genuine resonances. For the second and third cases (normal stromal tissue and prostate cancer, respectively) of the 300 total resonances, 273 were identified as spurious by their zero amplitudes and the pole-zero coincidences, yielding the 27 genuine resonances.

2.2.1 Padé reconstruction of the data from normal glandular prostate

The reconstructed data by the FPT$^{(-)}$ for the normal glandular prostate are presented in Table 4. These data are shown for partial signal lengths $N_P = 600$ and $N_P = 700$.

At the shorter signal length, $N_P = 600$ (upper panel (i)), 25 of the 27 resonances were identified. Peak #11 phosphocholine at 3.230242 ppm and the component of the taurine triplet at 3.250298 ppm (peak #13) were missing. The spectral parameters and concentrations were not fully exact for any of the resonances. The closest to being completely correct at $N_P = 600$ were the spectral parameters and calculated concentrations for the peaks at the outermost regions of the spectrum (peaks #1–8 and #25–27). The Padé-reconstructed chemical shift, Im(f_k) and calculated concentration

Table 1 Input spectral parameters and metabolite concentrations for normal glandular prostate derived from in vitro data of Ref. [42]. Hereafter, ppm denotes parts per million, au arbitrary units, M_k denotes metabolite assignment, C_k denotes concentration of M_k, while Lac denotes lactate, Ala alanine, Cit citrate, Cr creatine, PA polyamines, Cho choline, PC phosphocholine, GPC glycerophosphocholine, s-Ino scyllo-inositol, Tau taurine, m-Ino myoinositol

INPUT DATA (NORMAL GLANDULAR): SPECTRAL PARAMETERS, CONCENTRATIONS and METABOLITE ASSIGNMENTS

Phases of All Harmonics are set Equal to Zero: $\phi_k = 0$ (k = 1,..., K; K = 27)

N_k (Metabolite # k)	Re(f_k) (ppm)	Im(f_k) (ppm)	$\|d_k\|$ (au)	C_k(μM/g)	M_k (Assignment)
1	1.330148	0.013213	7.374199	40.3	Lac
2	1.490417	0.030361	1.579140	8.63	Ala
3	2.515197	0.008242	1.500457	8.20	Cit
4	2.540235	0.009624	2.616651	14.3	Cit
5	2.720146	0.010205	2.525160	13.8	Cit
6	2.750328	0.007014	1.244282	6.80	Cit
7	3.040309	0.006951	1.661482	9.08	Cr
8	3.100416	0.021432	2.104300	11.5	PA
9	3.140263	0.025760	1.280878	7.00	PA
10	3.210152	0.002367	0.644099	3.52	Cho
11	3.230242	0.010313	0.181153	0.99	PC
12	3.240318	0.003014	0.468435	2.56	GPC
13	3.250298	0.004362	0.384263	2.10	Tau
14	3.260429	0.005921	0.823422	4.50	Tau
15	3.275351	0.005671	0.219579	1.20	Tau
16	3.350137	0.007324	0.331199	1.81	s–Ino
17	3.420319	0.004290	0.201281	1.10	Tau
18	3.430241	0.005014	0.329369	1.80	Tau
19	3.440448	0.004721	0.182983	1.00	Tau
20	3.533243	0.006432	0.534309	2.92	m–Ino
21	3.550326	0.009324	1.557182	8.51	m–Ino
22	3.563639	0.007291	0.795974	4.35	m–Ino
23	3.626378	0.006952	0.589204	3.22	m–Ino
24	3.640411	0.009850	1.374199	7.51	m–Ino
25	3.655389	0.005812	0.444648	2.43	m–Ino
26	4.070235	0.012823	0.962489	5.26	m–Ino
27	4.120142	0.019891	1.134492	6.20	Lac

Table 2 Input spectral parameters and metabolite concentrations for normal stromal prostate derived from *in vitro* data of Ref. [42]

INPUT DATA (NORMAL STROMAL): SPECTRAL PARAMETERS, CONCENTRATIONS and METABOLITE ASSIGNMENTS

Phases of All Harmonics are set Equal to Zero: $\phi_k = 0$ (k = 1,..., K; K = 27)

N_k (Metabolite # k)	Re(f_k) (ppm)	Im(f_k) (ppm)	$\lvert d_k \rvert$ (au)	C_k(μM/g)	M_k (Assignment)
1	1.330148	0.013214	7.154620	39.1	Lac
2	1.490417	0.030360	1.244282	6.80	Ala
3	2.515197	0.010242	0.559927	3.06	Cit
4	2.540235	0.012151	0.977127	5.34	Cit
5	2.720146	0.012203	0.944190	5.16	Cit
6	2.750328	0.009014	0.464776	2.54	Cit
7	3.040309	0.006132	1.396157	7.63	Cr
8	3.100416	0.018432	0.345837	1.89	PA
9	3.140263	0.022761	0.230558	1.26	PA
10	3.210152	0.002613	0.495883	2.71	Cho
11	3.230242	0.010314	0.221409	1.21	PC
12	3.240318	0.005121	0.572736	3.13	GPC
13	3.250298	0.004132	0.329369	1.80	Tau
14	3.260429	0.003821	0.708143	3.87	Tau
15	3.275351	0.005670	0.188472	1.03	Tau
16	3.350137	0.005022	0.364135	1.99	s–Ino
17	3.420319	0.003690	0.175663	0.96	Tau
18	3.430241	0.003012	0.287283	1.57	Tau
19	3.440448	0.004123	0.159195	0.87	Tau
20	3.533243	0.006432	0.420860	2.30	m–Ino
21	3.550326	0.009324	1.225984	6.70	m–Ino
22	3.563639	0.007290	0.625801	3.42	m–Ino
23	3.626378	0.005951	0.462946	2.53	m–Ino
24	3.640411	0.007432	1.081427	5.91	m–Ino
25	3.655389	0.004814	0.351327	1.92	m–Ino
26	4.070235	0.010123	0.753888	4.12	m–Ino
27	4.120142	0.019891	1.097896	6.00	Lac

Table 3 Input spectral parameters and metabolite concentrations for prostate cancer derived from *in vitro* data of Ref. [42]

INPUT DATA (MALIGNANT): SPECTRAL PARAMETERS, CONCENTRATIONS and METABOLITE ASSIGNMENTS

Phases of All Harmonics are set Equal to Zero: $\phi_k = 0$ (k = 1,..., K; K = 27)

N_k (Metabolite # k)	$Re(f_k)$ (ppm)	$Im(f_k)$ (ppm)	$\lvert d_k \rvert$ (au)	C_k(μM/g)	M_k (Assignment)
1	1.330148	0.013213	11.07045	60.5	Lac
2	1.490417	0.030362	2.305581	12.6	Ala
3	2.515197	0.016240	0.680695	3.72	Cit
4	2.540235	0.020952	1.185727	6.48	Cit
5	2.720146	0.020204	1.152790	6.30	Cit
6	2.750328	0.018213	0.567246	3.10	Cit
7	3.040309	0.006951	1.780421	9.73	Cr
8	3.100416	0.021434	0.580055	3.17	PA
9	3.140263	0.032762	0.386093	2.11	PA
10	3.210152	0.002814	0.823422	4.50	Cho
11	3.230242	0.003952	1.235133	6.75	PC
12	3.240318	0.005890	0.473925	2.59	GPC
13	3.250298	0.004123	0.364135	1.99	Tau
14	3.260429	0.003141	0.781336	4.27	Tau
15	3.275351	0.005672	0.208600	1.14	Tau
16	3.350137	0.004324	0.459286	2.51	s–Ino
17	3.420319	0.003626	0.190302	1.04	Tau
18	3.430241	0.001426	0.312900	1.71	Tau
19	3.440448	0.003821	0.173833	0.95	Tau
20	3.533243	0.006434	0.548948	3.00	m–Ino
21	3.550326	0.010323	1.601098	8.75	m–Ino
22	3.563639	0.007291	0.817932	4.47	m–Ino
23	3.626378	0.005952	0.611162	3.34	m–Ino
24	3.640411	0.009434	1.425435	7.79	m–Ino
25	3.655389	0.004812	0.461116	2.52	m–Ino
26	4.070235	0.012421	0.993596	5.43	m–Ino
27	4.120142	0.012890	1.701738	9.30	Lac

Table 4 Padé-reconstructed spectral parameters and metabolite concentrations for normal glandular prostate with the input data as derived from Ref. [42]

CONVERGENCE of SPECTRAL PARAMETERS and CONCENTRATIONS in FPT$^{(-)}$: PARTIAL SIGNAL LENGTHS N_P = 600, 700

(i) Reconstructed Data (Normal Glandular) : N_P = 600 ; Missing Resonances : # 11 (PC) and # 13 (Tau)

N_k (Metabolite # k)	Re(f_k) (ppm)	Im(f_k) (ppm)	$\|d_k\|$ (au)	C_k (μM/g)	M_k (Assignment)
1	1.330148	0.013213	7.374172	40.3	Lac
2	1.490419	0.030353	1.577285	8.62	Ala
3	2.515197	0.008242	1.500502	8.20	Cit
4	2.540235	0.009624	2.616647	14.3	Cit
5	2.720146	0.010205	2.525202	13.8	Cit
6	2.750328	0.007014	1.244305	6.80	Cit
7	3.040309	0.006951	1.661438	9.08	Cr
8	3.100415	0.021427	2.103129	11.5	PA
9	3.140287	0.025772	1.282285	7.01	PA
10	3.210129	0.002369	0.643592	3.52	Cho
12	3.242549	0.011163	1.066128	5.83	GPC
14	3.262437	0.006985	0.865424	4.73	Tau
15	3.274335	0.005416	0.254324	1.39	Tau
16	3.350141	0.007318	0.330869	1.81	s–Ino
17	3.420373	0.004365	0.208105	1.14	Tau
18	3.430250	0.004800	0.313167	1.71	Tau
19	3.440350	0.004816	0.191041	1.04	Tau
20	3.533241	0.006444	0.535570	2.93	m–Ino
21	3.550328	0.009301	1.551185	8.48	m–Ino
22	3.563630	0.007305	0.799499	4.37	m–Ino
23	3.626376	0.006939	0.587325	3.21	m–Ino
24	3.640406	0.009865	1.377351	7.53	m–Ino
25	3.655393	0.005808	0.443946	2.43	m–Ino
26	4.070235	0.012823	0.962450	5.26	m–Ino
27	4.120142	0.019890	1.134339	6.20	Lac

(ii) Reconstructed Data (Normal Glandular) : N_P = 700 ; Converged (All Resonances Resolved)

N_k (Metabolite # k)	Re(f_k) (ppm)	Im(f_k) (ppm)	$\|d_k\|$ (au)	C_k (μM/g)	M_k (Assignment)
1	1.330148	0.013213	7.374199	40.3	Lac
2	1.490417	0.030361	1.579140	8.63	Ala
3	2.515197	0.008242	1.500457	8.20	Cit
4	2.540235	0.009624	2.616651	14.3	Cit
5	2.720146	0.010205	2.525160	13.8	Cit
6	2.750328	0.007014	1.244282	6.80	Cit
7	3.040309	0.006951	1.661482	9.08	Cr
8	3.100416	0.021432	2.104300	11.5	PA
9	3.140263	0.025760	1.280878	7.00	PA
10	3.210152	0.002367	0.644099	3.52	Cho
11	3.230242	0.010313	0.181153	0.99	PC
12	3.240318	0.003014	0.468435	2.56	GPC
13	3.250298	0.004362	0.384263	2.10	Tau
14	3.260429	0.005921	0.823422	4.50	Tau
15	3.275351	0.005671	0.219579	1.20	Tau
16	3.350137	0.007324	0.331199	1.81	s–Ino
17	3.420319	0.004290	0.201281	1.10	Tau
18	3.430241	0.005014	0.329369	1.80	Tau
19	3.440448	0.004721	0.182983	1.00	Tau
20	3.533243	0.006432	0.534309	2.92	m–Ino
21	3.550326	0.009324	1.557182	8.51	m–Ino
22	3.563639	0.007291	0.795974	4.35	m–Ino
23	3.626378	0.006952	0.589204	3.22	m–Ino
24	3.640411	0.009850	1.374199	7.51	m–Ino
25	3.655389	0.005812	0.444648	2.43	m–Ino
26	4.070235	0.012823	0.962489	5.26	m–Ino
27	4.120142	0.019891	1.134492	6.20	Lac

for lactate at 1.330148 ppm were all exact at $N_P = 600$, although the $|d_k|$ was correct only to 4 of the 6 decimal places. The last digit of the chemical shift and two digits of Im(f_k) were not exact for alanine, only two of the 6 decimal places were correct for the $|d_k|$ and its calculated concentration was correct only to 1 decimal place at $N_P = 600$. For each of the doublets of doublets of citrate and for creatine the chemical shift,

Im(f_k) and concentrations were exact, although the $|d_k|$'s were only correct to 3 or 4 of the six decimal places at $N_P = 600$. The polyamine resonance peak #8 had fully correct calculated concentration, although the chemical shift, Im(f_k) and $|d_k|$ were correct to 5, 4 and 2 decimal places, respectively at $N_P = 600$. Note that all the input concentrations are given with at most two decimals to preserve the accuracy of the corresponding data from Ref. [42]. The presently reported concentrations are set to match this latter input, but all the reconstructed parameters are listed with 6 decimals.

Within the spectrally denser region from 3.14 to 3.65 ppm, none of the reconstructed spectral parameters of the identified resonances were fully exact at $N_P = 600$, although the calculated concentrations of choline, scyllo-inositol and the component within the myoinositol triplet centered at 3.6555394 ppm were correct. At $N_P = 600$ the chemical shift, Im(f_k) and calculated concentration of the myoinositol singlet at 4.070235 ppm were fully correct, but the $|d_k|$ was not. The Re(f_k) of the lactate peak (#27) was correctly reconstructed to be 4.120142 ppm and the calculated concentration was also correct, but for the Im(f_k) and $|d_k|$ the last one and three decimal places, respectively were not exact at $N_P = 600$. Although most of the calculated concentrations had the correct integer values, this was not the case for GPC. Instead of the correct concentration of 2.56 μM/g, the concentration of GPC was calculated to be 5.83 μM/g, at $N_P = 600$, and the reconstructed $|d_k|$ was 1.066128 whereas the correct value was 0.468435.

At $N_P = 700$ full convergence was attained for all the reconstructed parameters and calculated concentrations for each of the 27 resonances (bottom panel (ii) of Table 4). The stability of convergence was confirmed at higher partial signal lengths and at the total signal length $N = 1024$.

Figure 1 shows the absorption component shape spectra reconstructed by the FPT$^{(-)}$ at the two partial signal lengths: $N_P = 54$ and $N_P = 800$ for the normal glandular prostate data. At $N_P = 54$, fifteen of the twenty-seven resonances were missing (top panel). Only at the two extremes of the spectrum were all the resonances resolved and with heights that were nearly correct (lactate and alanine at 1.33 and 1.49 ppm respectively and myoinositol and lactate at about 4.07 and 4.12 ppm, respectively). Within the relatively denser spectral region from ∼2.5 to 3.70 ppm, only eight of the twenty-three peaks were resolved and an admixture of the absorption and dispersive modes can be observed, the latter including structures with negative intensities on the ordinate axis. Moreover, the relative heights of the doublet citrate peak near 2.5 ppm are reversed, i.e. the peak at about 2.52 ppm is larger than the one at about 2.54 ppm. The second citrate peak near 2.75 ppm appears as a singlet, when it should be a doublet. Similarly the peaks near 3.55 and 3.65 ppm corresponding to myoinositol appear as singlets, when they should be triplets. There are three broad peaks at ∼3.05, 3.22 and 3.3 ppm, when there should be ten peaks within that spectral region. These three broad peaks all have notable dispersive features with negative intensities. In the bottom panel of Fig. 1 at $N_P = 800$, all 27 resonances were resolved with correct peak heights including all the multiplet resonances and the overlapping resonances of phosphocholine at 3.23 ppm and glycerophosphocholine at 3.24 ppm. At $N_P = 800$ the dispersive modes are absent.

We present the case with $N_P = 54$ because this is the least number of signal points which is theoretically needed to resolve 27 resonances (27 unknown frequencies and

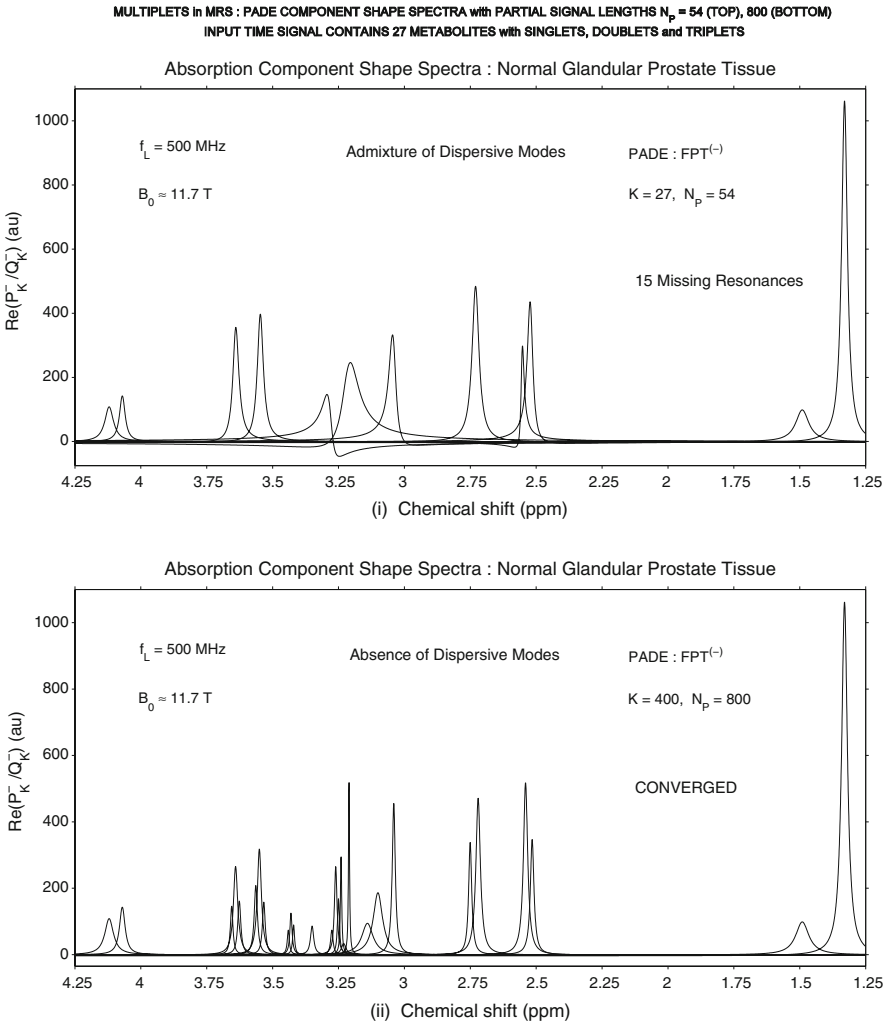

Fig. 1 Convergence pattern for the Padé-reconstructed absorption component spectra (top panel) for normal glandular prostate, from in vitro data of Ref. [42]. At $N_P = 54$ (top panel (i)) 15 of the 27 resonances are missing. At $N_P = 800$ (bottom panel (ii)) all 27 resonances are resolved. Convergence of the absorption component spectra remains stable at higher N_P including the full signal length N

27 unknown amplitudes considered in concert require 54 linear equations). However, it is seen from panel (i) of Fig. 1 that this algebraic condition of completeness ($N_P = 2K = 2 \times 27$) is totally insufficient, primarily due to the high density of states. In practice, not $2K$ but more than $10K$ signal points are needed for complicated, densely packed spectra.

The total absorption shape spectra reconstructed by the FPT$^{(-)}$ at the same two partial signal lengths $N_P = 54$ (top panel (i)) and $N_P = 800$ (bottom panel (ii)) for the normal glandular prostate data are shown in Fig. 2. Similarly to the component shape spectra at $N_P = 54$, the relative heights of the doublet citrate peak near 2.5 ppm

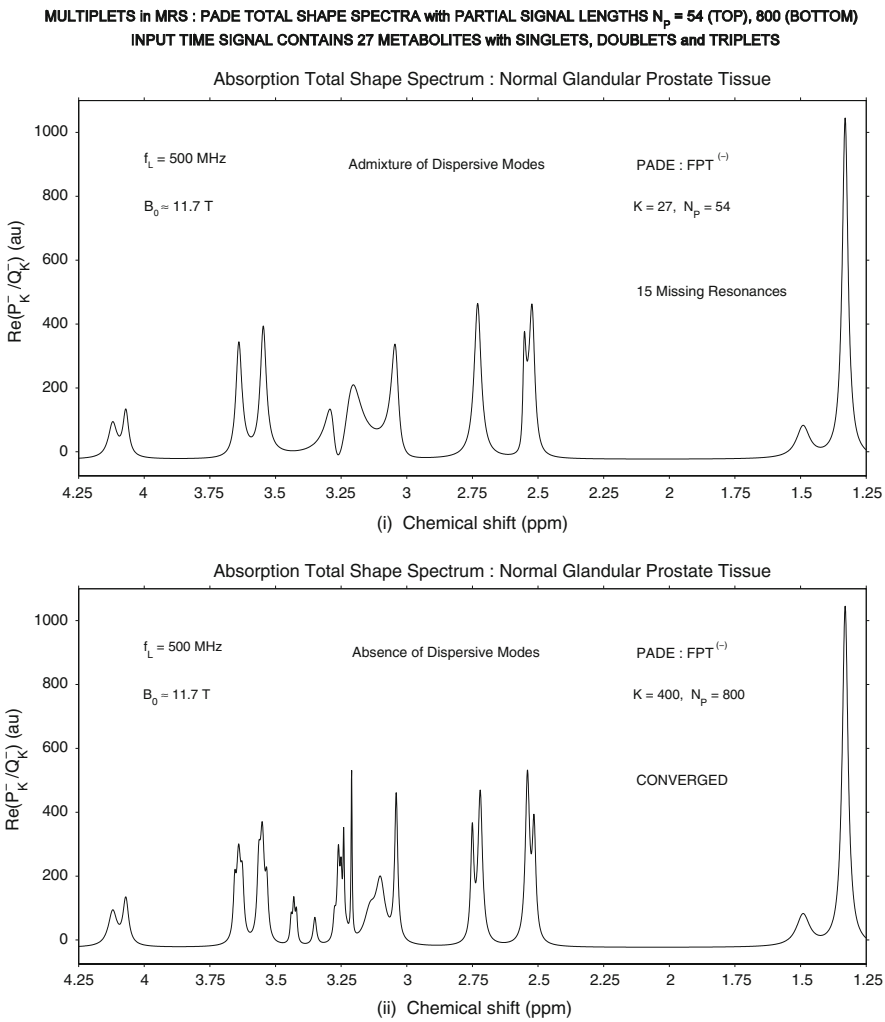

Fig. 2 Padé-reconstructed absorption total shape spectra for normal glandular prostate, from in vitro data of Ref. [42]. The upper panel (i) is at $N_P = 54$ and the converged spectrum at $N_P = 800$ is shown in the bottom panel (ii)

are reversed, i.e. the peak at around 2.52 ppm is larger than the one at 2.54 ppm, and the second citrate peak near 2.75 ppm appears as a singlet, when it should be a doublet. The peaks near 3.55 and 3.65 ppm corresponding to myoinositol, appear as singlets, when they should be triply serrated. Only those resonances in the two extremes of the total shape spectrum were reconstructed to approximately their correct heights and widths (lactate and alanine at 1.33 and 1.49 ppm respectively and myoinositol and lactate at ∼4.07 ppm and 4.12 ppm, respectively). The admixture of the absorption and dispersive mode is seen in the region between ∼3.05 and 3.3 ppm, reflected in the appearance of three peaks that are broadened with lowered heights and upward

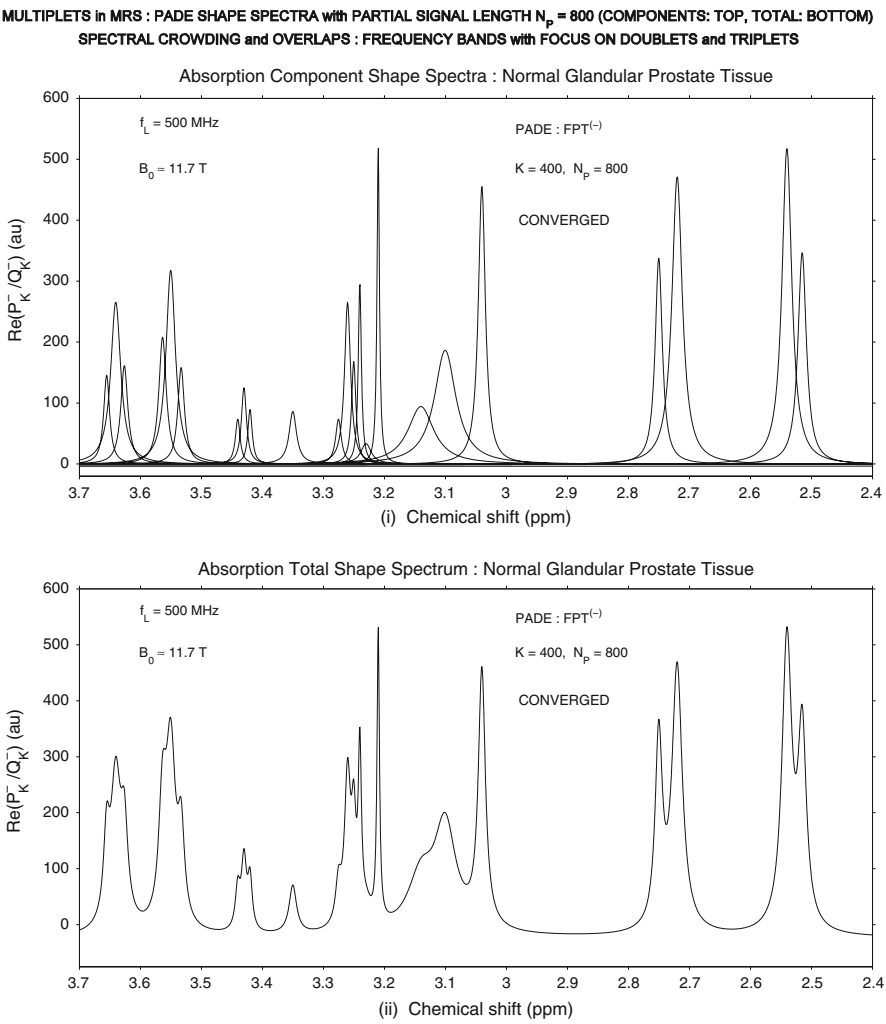

Fig. 3 Converged Padé-reconstructed absorption component shape spectra (top panel (i)) and converged absorption total shape spectra (bottom panel (ii)) for normal glandular prostate, from in vitro data of Ref. [42]

distortion (non-Lorentziau peaks). The converged total absorption shape spectrum at $N_P = 800$ is seen in the bottom panel of Fig. 2, without any dispersive modes. Note that positive definiteness is not required for an absorption spectrum even when converged (see e.g. Fig. 2 (ii)).

In Fig. 3 the converged absorption component shape spectrum (top panel (i)) and total absorption shape spectrum (bottom panel (ii)) at $N_P = 800$ are compared within the zoomed region from 2.40 ppm to 3.70 ppm. Here, it can be seen that PC at 3.23 ppm and GPC at 3.24 ppm are completely resolved in the component shape spectrum, but only a single peak appears on the total shape spectrum. From the total shape spectrum it

can only be surmised that e.g. the peaks assigned to myoinositol with three serrations centered respectively at ∼3.55 and 3.66 ppm are triplets. In the component shape spectrum, reconstructed from the spectral parameters that were exactly calculated via the FPT$^{(-)}$ it is confirmed that indeed there are precisely three overlapping components at both of these chemical shift frequencies. Similarly, the two triply serrated peaks centered at ∼3.43 and 3.26 ppm corresponding to taurine on the total shape spectrum, are shown in panel (i) to be comprised of three components each. For the latter case, centered at ∼3.26 ppm, this would be nearly impossible to know with any certainty from the total shape spectrum, which towards the right-hand side is very close to the GPC and PC peaks. It would also be difficult to know with certainty from the total shape spectrum that the broad structure with a prominent peak centered at about 3.1 ppm is comprised of exactly two components that correspond to polyamine.

2.2.2 Padé reconstruction of the data from normal stromal prostate

The reconstructed data by the FPT$^{(-)}$ for the normal stromal prostate are presented in Table 5. These data are shown for partial signal lengths $N_P = 500$ and $N_P = 600$.

The pattern of the reconstructed findings at the shorter signal length $N_P = 500$ (upper panel (i)) for the normal stromal tissue was fairly similar to that described for the normal glandular prostate data. Again, the two resonances, peak#11 phosphocholine at 3.230242 ppm and the component of the taurine triplet at 3.250298 ppm (peak #13), were missing.

At $N_P = 500$ peak #1 (lactate) and peak #5 of the citrate doublet were the only resonances for which all reconstructed spectral parameters and concentrations were fully exact on panel (i). The other resonances that were closest to being completely correct at $N_P = 500$ were mainly the spectral parameters and calculated concentrations at the outermost regions of the spectrum (peaks #2, 3, 5–7 and peaks #25–27). For alanine (peak #2) other than the last two digits of the $|d_k|$'s all the spectral parameters and calculated concentration were exact at $N_P = 500$. For the other components of the doublets of doublets of citrate and for creatine (peak #7) the chemical shift, Im(f_k) and concentrations were exact and the $|d_k|$'s were correct to 4 or 5 of the six decimal places at $N_P = 500$. The polyamine resonance at 3.100416 ppm had fully correct calculated concentration, and the reconstructed chemical shift, whereas Im(f_k) and $|d_k|$ were correct to 5, 5 and 4 decimal places, respectively at $N_P = 500$.

Within the spectrally denser region from 3.14 to 3.65 ppm, again none of the reconstructed spectral parameters of the identified resonances were fully exact at $N_P = 500$. However, the calculated concentrations of scyllo-inositol (peak #16) and peaks #23–25 that were the components of one of the myoinositol triplets were correct. At $N_P = 500$ the chemical shift, Im(f_k) and calculated concentration of peak #26, the myoinositol singlet at 4.070235 ppm were fully correct, but the last digit of the $|d_k|$ was not. The Re(f_k) and Im(f_k) of the lactate peak #27 were exactly reconstructed and the calculated concentration was also correct, but for $|d_k|$ the last two decimal places were not exact at $N_P = 500$.

Although most of the calculated concentrations had the correct integer values, this was not the case for the two peaks immediately adjacent to the missed resonances GPC (peak#12) and taurine (peak#14) which were both overestimated. Instead of the

Table 5 Padé-reconstructed spectral parameters and metabolite concentrations for normal stromal prostate with the input data as derived from Ref. [42]

CONVERGENCE of SPECTRAL PARAMETERS and CONCENTRATIONS in FPT$^{(-)}$: PARTIAL SIGNAL LENGTHS N_P = 500, 600

(i) Reconstructed Data (Normal Stromal) : N_P = 500 ; Missing Resonances : # 11 (PC) and # 13 (Tau)

N_k (Metabolite # k)	Re(f_k) (ppm)	Im(f_k) (ppm)	$\|d_k\|$ (au)	C_k (μM/g)	M_k (Assignment)
1	1.330148	0.013214	7.154620	39.1	Lac
2	1.490417	0.030360	1.244279	6.80	Ala
3	2.515197	0.010242	0.559928	3.06	Cit
4	2.540235	0.012151	0.977128	5.34	Cit
5	2.720146	0.012203	0.944190	5.16	Cit
6	2.750328	0.009014	0.464780	2.54	Cit
7	3.040309	0.006132	1.396156	7.63	Cr
8	3.100411	0.018433	0.345788	1.89	PA
9	3.140292	0.022726	0.229955	1.26	PA
10	3.210122	0.002639	0.498355	2.72	Cho
12	3.240382	0.010395	1.112238	6.08	GPC
14	3.261970	0.004502	0.765134	4.18	Tau
15	3.273710	0.005855	0.266296	1.46	Tau
16	3.350145	0.005025	0.364284	1.99	s–Ino
17	3.420144	0.003587	0.165519	0.91	Tau
18	3.430355	0.003221	0.304644	1.66	Tau
19	3.440427	0.003932	0.153322	0.84	Tau
20	3.533254	0.006419	0.420171	2.30	m–Ino
21	3.550303	0.009344	1.228695	6.71	m–Ino
22	3.563658	0.007292	0.624220	3.41	m–Ino
23	3.626374	0.005949	0.462618	2.53	m–Ino
24	3.640413	0.007434	1.081656	5.91	m–Ino
25	3.655388	0.004813	0.351285	1.92	m–Ino
26	4.070235	0.010123	0.753887	4.12	m–Ino
27	4.120142	0.019891	1.097886	6.00	Lac

(ii) Reconstructed Data (Normal Stromal) : N_P = 600 ; Converged (All Resonances Resolved)

N_k (Metabolite # k)	Re(f_k) (ppm)	Im(f_k) (ppm)	$\|d_k\|$ (au)	C_k (μM/g)	M_k (Assignment)
1	1.330148	0.013214	7.154620	39.1	Lac
2	1.490417	0.030360	1.244282	6.80	Ala
3	2.515197	0.010242	0.559927	3.06	Cit
4	2.540235	0.012151	0.977127	5.34	Cit
5	2.720146	0.012203	0.944190	5.16	Cit
6	2.750328	0.009014	0.464776	2.54	Cit
7	3.040309	0.006132	1.396157	7.63	Cr
8	3.100416	0.018432	0.345837	1.89	PA
9	3.140263	0.022761	0.230558	1.26	PA
10	3.210152	0.002613	0.495883	2.71	Cho
11	3.230242	0.010314	0.221409	1.21	PC
12	3.240318	0.005121	0.572736	3.13	GPC
13	3.250298	0.004132	0.329369	1.80	Tau
14	3.260429	0.003821	0.708143	3.87	Tau
15	3.275351	0.005670	0.188472	1.03	Tau
16	3.350137	0.005022	0.364135	1.99	s–Ino
17	3.420319	0.003690	0.175663	0.96	Tau
18	3.430241	0.003012	0.287283	1.57	Tau
19	3.440448	0.004123	0.159195	0.87	Tau
20	3.533243	0.006432	0.420860	2.30	m–Ino
21	3.550326	0.009324	1.225984	6.70	m–Ino
22	3.563639	0.007290	0.625801	3.42	m–Ino
23	3.626378	0.005951	0.462946	2.53	m–Ino
24	3.640411	0.007432	1.081427	5.91	m–Ino
25	3.655389	0.004814	0.351327	1.92	m–Ino
26	4.070235	0.010123	0.753888	4.12	m–Ino
27	4.120142	0.019891	1.097896	6.00	Lac

correct concentration of 3.13 μM/g, the concentration of GPC was calculated to be 6.08 μM/g, at $N_P = 500$ and the reconstructed $|d_k|$ was 1.112238 whereas the correct value was 0.572736. The concentration of the taurine peak #14 was calculated as 4.18 μM/g at $N_P = 500$, while 3.87 μM/g is the correct value.

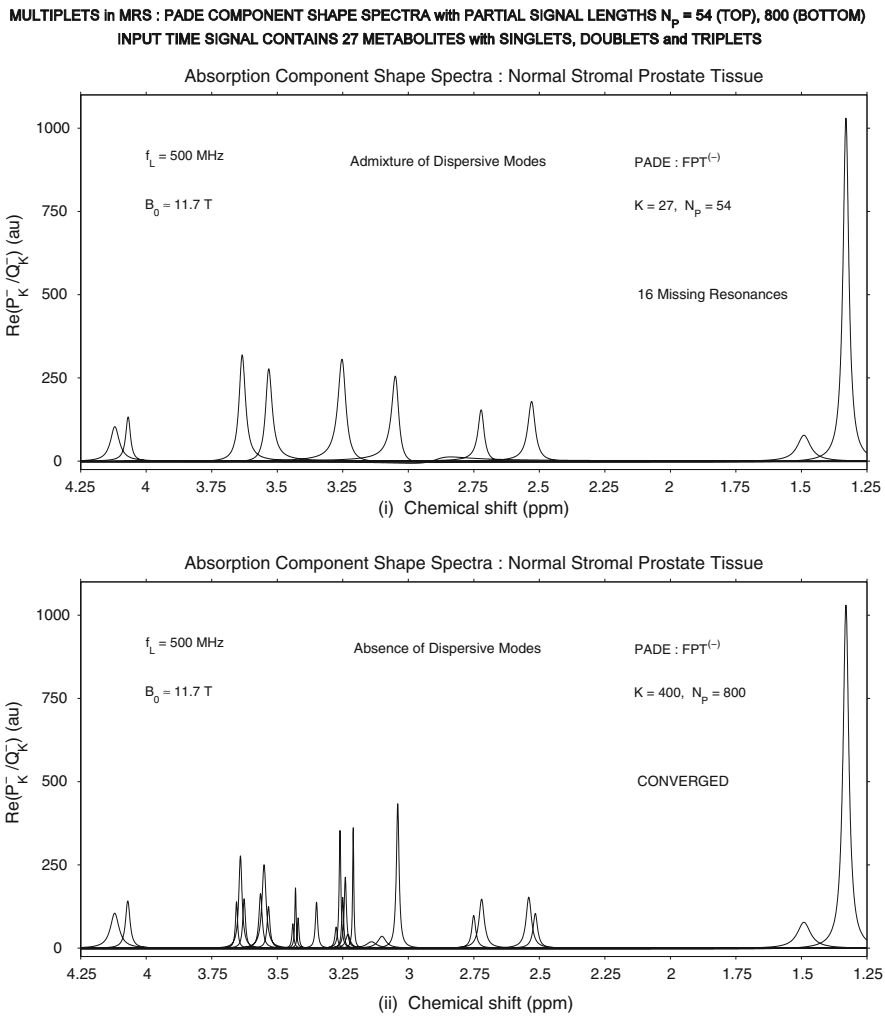

Fig. 4 Convergence pattern for the Padé-reconstructed absorption component spectra (top panel) for normal stromal prostate, from in vitro data of Ref. [42]. At $N_P = 54$ (top panel (i)) 16 of the 27 resonances are missing. At $N_P = 800$ (bottom panel (ii)) all 27 resonances are resolved. Convergence of the absorption component spectra remains stable at higher N_P including the full signal length N

At $N_P = 600$ full convergence was achieved for all the reconstructed parameters and calculated concentrations for all 27 resonances (bottom panel (ii) of Table 5). At higher partial signal length and the full signal length N all the reconstructed spectral parameters and calculated concentrations remained stable.

The Padé-reconstructed absorption component shape spectra at $N_P = 54$ and $N_P = 800$ for the normal stromal prostate data are displayed in Fig. 4. Sixteen of the 27 peaks were missing at $N_P = 54$ (upper panel (i)). Similarly to the pattern seen for normal glandular prostate, here at $N_P = 54$ for the normal stromal tissue, it was only at the two extremes of the spectrum that all the resonances were resolved and with heights

that were nearly correct (lactate and alanine at 1.33 and 1.49 ppm respectively and myoinositol and lactate at 4.07 and 4.12 ppm, respectively). From ∼2.5 to 3.65 ppm which was the relatively denser spectral region, only seven of the twenty-three peaks were resolved and some admixture of the absorption and dispersive modes is seen. The citrate doublet expected near 2.5 ppm appeared as a singlet. The citrate doublet near 2.75 ppm appears mainly as a singlet but there is also a broad component with very small amplitude centered around 2.8 ppm. The peaks near 3.55 and 3.65 ppm corresponding to myoinositol appear as singlets, when they should triplets. Within the spectral region between 3.0 and 3.35 ppm, there should be ten peaks, but only two peaks appear: one at ∼3.10 ppm and the other at ∼3.25 ppm.

The bottom panel (ii) of Fig. 4 at $N_P = 800$ shows all 27 resonances as being resolved with the correct peak heights. This includes all the multiplets as well as the overlapping resonances of phosphocholine at ∼3.23 ppm and glycerophosphocholine at ∼3.24 ppm. The dispersive modes are absent at this converged partial signal length.

Figure 5 shows the total absorption shape spectra reconstructed by the FPT$^{(-)}$ at the same two partial signal lengths: $N_P = 54$ (top panel (i)) and $N_P = 800$ (bottom panel (ii)) for the normal stromal prostate. As could be expected from the component spectrum, at $N_P = 54$ the structures at the two extremes of the spectrum were resolved and with heights that were approximately correct (lactate and alanine at 1.33 and 1.49 ppm respectively and myoinositol and lactate at 4.07 and 4.12 ppm, respectively). However, the peaks near 2.5 ppm appear as a singlet at $N_P = 54$, when they should have a double serration. A very low amplitude broad protuberance appears around 2.85 ppm, which is asymmetrically higher towards the right side. The creatine peak centered at around 3.05 ppm is broadened and of lower amplitude compared to the peak corresponding to creatine on the converged total shape spectrum. There is a single peak centered at 3.25 ppm at $N_P = 54$ instead of 4 very narrow peaks and a serrated structure to the left. The peaks at 3.35 ppm corresponding to scyllo-inositol and the triply serrated structure corresponding to taurine center at 3.43 ppm are completely absent on the total shape spectrum at $N_P = 54$. The two structures centered near 3.56 ppm and at 3.64 ppm corresponding to myoinositol are single peaks, whereas they should appear with triple serration. The low amplitude protuberances corresponding to polyamines that should appear at around 3.10 and 3.14 ppm are completely absent. However, the total absorption shape spectrum at $N_P = 800$ for normal stromal prostate shown in the bottom panel of Fig. 5 converged. This is consistent with the component shape spectrum which resolved all the 27 resonances by retrieving all the exact spectral parameters.

In Fig. 6 for the normal stromal prostate, the converged absorption component shape spectrum (top panel (i)) and total absorption shape spectrum (bottom panel (i)) at $N_P = 800$ are compared within the expanded region from 2.40 to 3.70 ppm. Similarly to the previous case of normal glandular prostate, here as well it can be seen that PC at 3.23 ppm and GPC at 3.24 ppm are completely resolved in the component shape spectrum, but only a single peak appears on the total shape spectrum. Again, although the triply and doubly serrated peaks seen on the total shape spectrum could suggest the number of components, it is only from the converged component spectrum that actual number of resonances reconstructed via the FPT$^{(-)}$ can

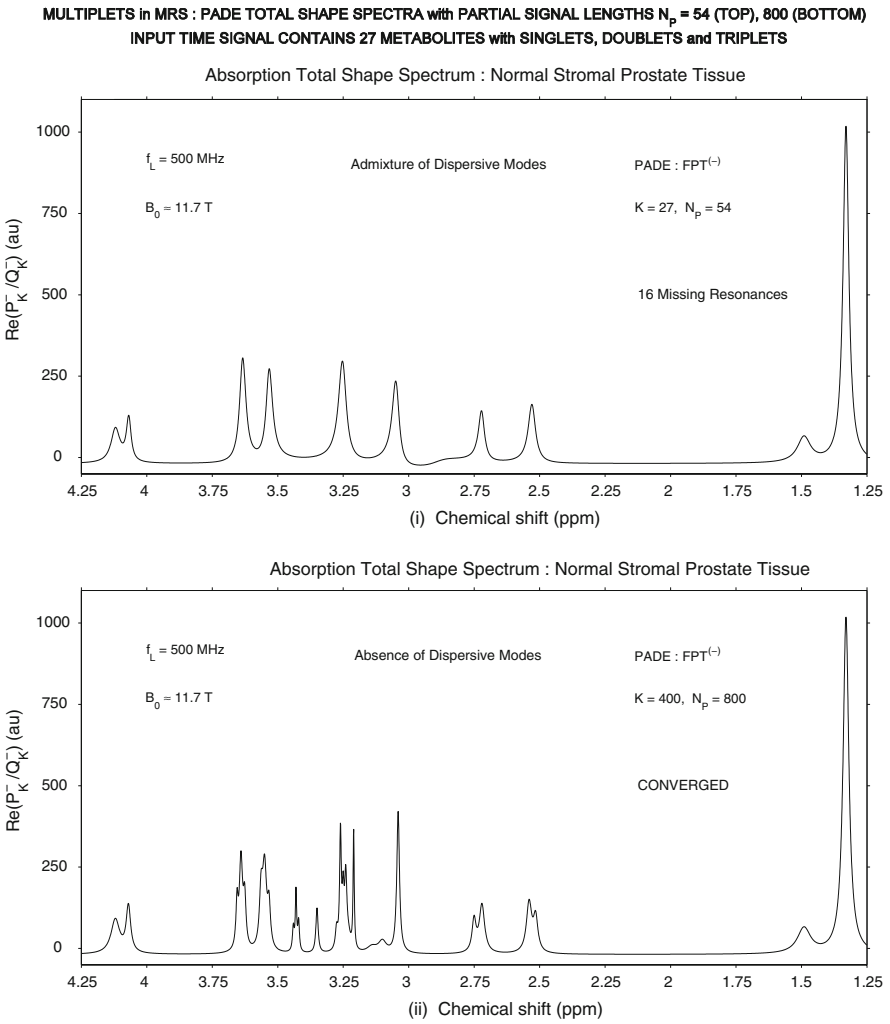

Fig. 5 Padé-reconstructed absorption total shape spectra for normal stromal prostate, from in vitro data of Ref. [42]. The upper panel (i) is at $N_P = 54$ and the converged spectrum at $N_P = 800$ is shown in the bottom panel (ii)

be determined with confidence. Since the polyamine peaks are very low in the normal stromal prostate, it would be even more difficult than for the glandular case to determine from the total shape spectrum that there are indeed exactly two PA components.

2.2.3 Padé reconstruction of the data from malignant prostate

The reconstructed data by the FPT$^{(-)}$ for prostate cancer are presented in Table 6. These data are shown for partial signal lengths $N_P = 500$ and $N_P = 600$. Prior to

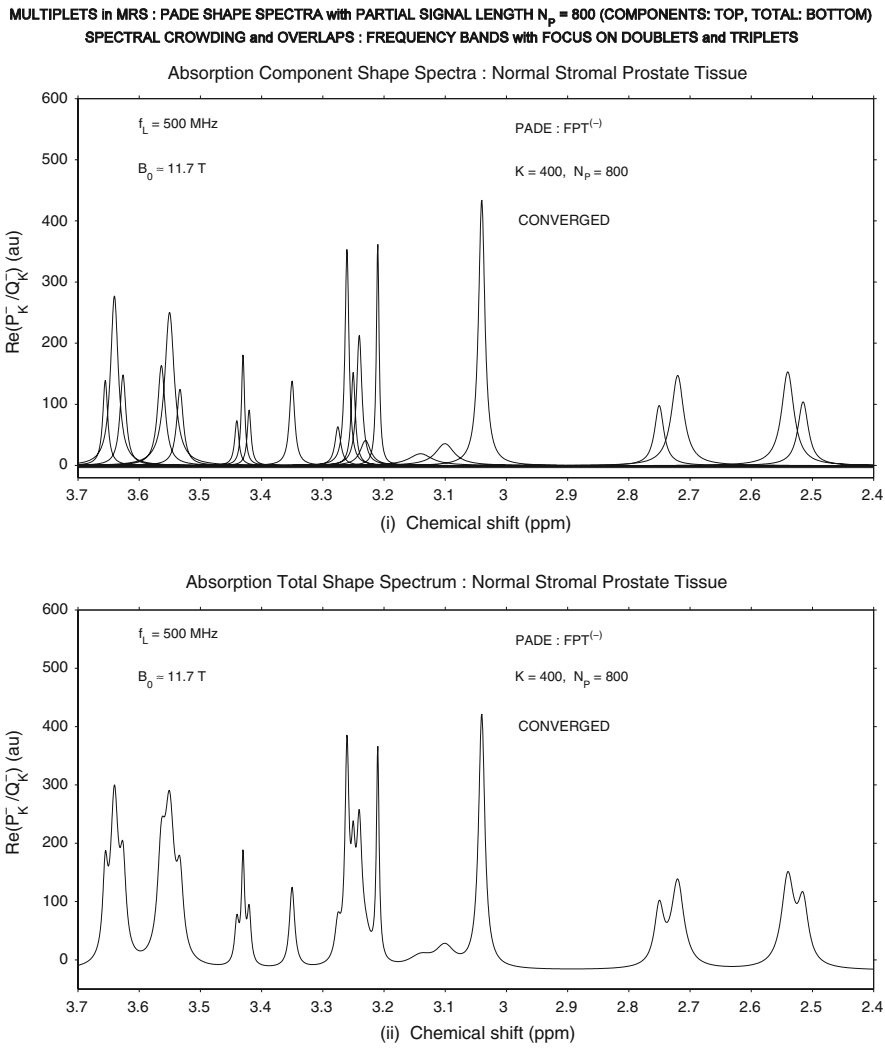

Fig. 6 Converged Padé-reconstructed absorption component shape spectra (top panel (i)) and converged absorption total shape spectra (bottom panel (ii)) for normal stromal prostate, from in vitro data of Ref. [42]

convergence, at $N_P = 500$ (upper panel (i)), 26 of the 27 resonances were identified. The missing resonance at $N_P = 500$ was the component of the taurine triplet at 3.250298 ppm (peak #13).

The calculated concentrations for resonances # 1–8 and #23–27 were completely correct at $N_P = 500$ and the all spectral parameters were fully exact for lactate at 1.330148 ppm (peak #1) and at 4.12042 (peak #27), as well as for the myoinositol singlet (peak #26) at 4.079235 ppm. For the components of the myoinositol triplet (peaks #23–25) the reconstructed chemical shifts, $\mathrm{Im}(f_k)$ and $|d_k|$ were either fully correct or correct to 3–5 of the six decimal places (accounting for round-off). The

Table 6 Padé-reconstructed spectral parameters and metabolite concentrations for malignant prostate with the input data as derived from Ref. [42]

CONVERGENCE of SPECTRAL PARAMETERS and CONCENTRATIONS in FPT$^{(-)}$: PARTIAL SIGNAL LENGTHS N_P = 500, 600

(i) Reconstructed Data (Malignant) : N_P = 500 ; Missing Resonance : # 13 (Tau)

N_k (Metabolite # k)	Re(f_k) (ppm)	Im(f_k) (ppm)	$\|d_k\|$ (au)	C_k (μM/g)	M_k (Assignment)
1	1.330148	0.013213	11.07045	60.5	Lac
2	1.490417	0.030362	2.305586	12.6	Ala
3	2.515197	0.016240	0.680689	3.72	Cit
4	2.540235	0.020952	1.185733	6.48	Cit
5	2.720146	0.020204	1.152776	6.30	Cit
6	2.750328	0.018213	0.567253	3.10	Cit
7	3.040309	0.006951	1.780424	9.73	Cr
8	3.100418	0.021437	0.580318	3.17	PA
9	3.140233	0.032708	0.384660	2.10	PA
10	3.210153	0.002834	0.829223	4.53	Cho
11	3.229878	0.004204	1.252506	6.84	PC
12	3.246399	0.012406	0.950890	5.20	GPC
14	3.261533	0.002729	0.625188	3.42	Tau
15	3.274760	0.006965	0.288772	1.58	Tau
16	3.350140	0.004321	0.458939	2.51	s–Ino
17	3.420142	0.003723	0.187071	1.02	Tau
18	3.430390	0.001404	0.309790	1.69	Tau
19	3.440276	0.003813	0.180274	0.98	Tau
20	3.533235	0.006428	0.547676	2.99	m–Ino
21	3.550337	0.010342	1.605352	8.77	m–Ino
22	3.563644	0.007281	0.815504	4.46	m–Ino
23	3.626378	0.005954	0.611484	3.34	m–Ino
24	3.640413	0.009432	1.424954	7.79	m–Ino
25	3.655388	0.004812	0.461176	2.52	m–Ino
26	4.070235	0.012421	0.993596	5.43	m–Ino
27	4.120142	0.012890	1.701738	9.30	Lac

(ii) Reconstructed Data (Malignant) : N_P = 600 ; Converged (All Resonances Resolved)

N_k (Metabolite # k)	Re(f_k) (ppm)	Im(f_k) (ppm)	$\|d_k\|$ (au)	C_k (μM/g)	M_k (Assignment)
1	1.330148	0.013213	11.07045	60.5	Lac
2	1.490417	0.030362	2.305581	12.6	Ala
3	2.515197	0.016240	0.680695	3.72	Cit
4	2.540235	0.020952	1.185727	6.48	Cit
5	2.720146	0.020204	1.152790	6.30	Cit
6	2.750328	0.018213	0.567246	3.10	Cit
7	3.040309	0.006951	1.780421	9.73	Cr
8	3.100416	0.021434	0.580055	3.17	PA
9	3.140263	0.032762	0.386093	2.11	PA
10	3.210152	0.002814	0.823422	4.50	Cho
11	3.230242	0.003952	1.235133	6.75	PC
12	3.240318	0.005890	0.473925	2.59	GPC
13	3.250298	0.004123	0.364135	1.99	Tau
14	3.260429	0.003141	0.781336	4.27	Tau
15	3.275351	0.005672	0.208600	1.14	Tau
16	3.350137	0.004324	0.459286	2.51	s–Ino
17	3.420319	0.003626	0.190302	1.04	Tau
18	3.430241	0.001426	0.312900	1.71	Tau
19	3.440448	0.003821	0.173833	0.95	Tau
20	3.533243	0.006434	0.548948	3.00	m–Ino
21	3.550326	0.010323	1.601098	8.75	m–Ino
22	3.563639	0.007291	0.817932	4.47	m–Ino
23	3.626378	0.005952	0.611162	3.34	m–Ino
24	3.640411	0.009434	1.425435	7.79	m–Ino
25	3.655389	0.004812	0.461116	2.52	m–Ino
26	4.070235	0.012421	0.993596	5.43	m–Ino
27	4.120142	0.012890	1.701738	9.30	Lac

chemical shifts and Im(f_k) were exactly reconstructed for alanine, the doublets of citrate doublets and creatine, and the $|d_k|$'s for these resonances were correct to 4–5 of the six decimal places. For peaks #9 and #10 (polyamine and choline, respectively), the concentrations were exact to 1 decimal place.

At $N_P = 500$ the concentration of phosphocholine (peak #11) was of the correct integer but the spectral parameters were correct to only 1–3 decimal places. For GPC

(peak #12) the concentration was overestimated by about a factor of 2. The concentration of the taurine component (peak #14) was underestimated by approximately 20% at $N_P = 500$. The concentration of the singlet scyllo-inositol (peak #16) was fully correct. Peaks #15 and #17–19, components of the two taurine triplets, had the correct integer values for the concentrations at $N_P = 500$. The concentrations of the components of the myoinositol triplet (peaks # 20–22) were correct to at least one of two decimal places (accounting for round-off).

At $N_P = 600$ full convergence was achieved for all the exactly reconstructed parameters for each of the 27 resonances (lower panel (ii) of Table 6). As with the

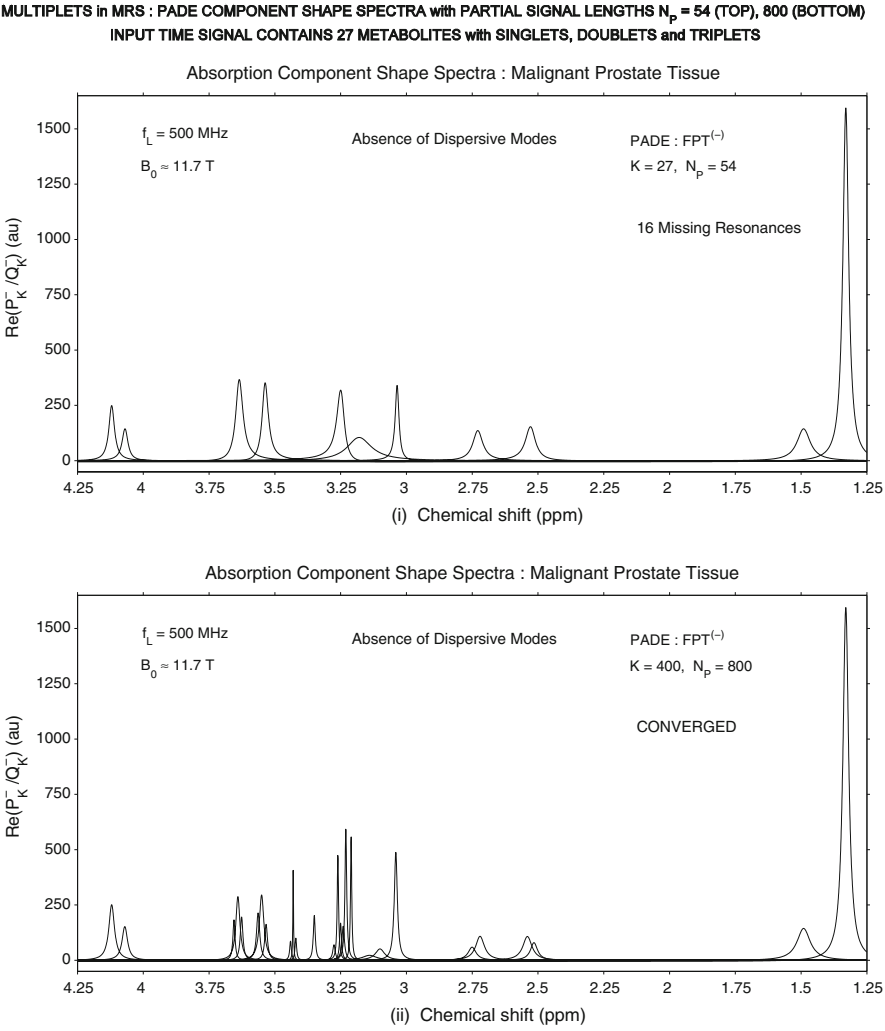

Fig. 7 Convergence pattern for the Padé-reconstructed absorption component spectra (top panel) for cancerous prostate, from in vitro data of Ref. [42]. At $N_P = 54$ (top panel (i)) only 11 of the 27 resonances are identified. At $N_P = 800$ (bottom panel (ii)) all 27 resonances are resolved. Convergence of the absorption component spectra remains stable at higher N_P including the full signal length N

other two cases, stability of convergence was found at higher partial signal length and at the full signal length N.

The Padé-reconstructed absorption component shape spectra at $N_P = 54$ and $N_P = 800$ for the prostate cancer data are presented in Fig. 7. Of the 27 peaks, only 11 were resolved at $N_P = 54$ (upper panel (i)). As was the case for normal glandular and stromal prostate, here at $N_P = 54$ for the malignant prostate spectra, only at the two extremes of the spectrum were all the resonances resolved and with heights that were nearly correct for lactate and alanine at 1.33 and 1.49 ppm and myoinositol and lactate at 4.07 and 4.12 ppm. In the relatively denser spectral region from ∼2.5 to 3.65 ppm, altogether 7 of the 23 peaks were resolved but there were no dispersive modes as in the other two cases (normal glandular and normal stromal prostate). There were singlets near 2.5 and 2.75 ppm, whereas there should be doublets of citrate at each of those regions. The peaks near 3.55 and 3.65 ppm corresponding to myoinositol appear as singlets, when they should be triplets. While there should be 10 peaks between 3.0 and 3.35 ppm, only three peaks appear. In the bottom panel (ii) of Fig. 7 at $N_P = 800$, all 27 resonances were resolved with the correct peak heights, widths, positions and zero phases. This includes all the multiplet resonances as well as PC and GPC.

The total absorption shape spectra reconstructed by the $\mathrm{FPT}^{(-)}$ at the same two partial signal lengths $N_P = 54$ (top panel (i)) and $N_P = 800$ (bottom panel (ii)) for malignant prostate are displayed in Fig. 8. At $N_P = 54$ lactate and alanine at 1.33 and 1.49 ppm and myoinositol and lactate at 4.07 and 4.12 ppm were resolved and with heights that were nearly correct, as was the case for component absorption spectrum for malignant prostate data. The citrate peaks near 2.5 and 2.75 ppm appear single and narrower at $N_P = 54$, than on the converged total shape spectrum. The creatine peak centered at around 3.05 ppm is also broadened and has a lower amplitude compared to the peak corresponding to creatine on the converged total shape spectrum. There is a single peak centered at 3.25 ppm at $N_P = 54$ instead of the two very narrow peaks and a triply serrated structure to the left. The peaks at 3.35 ppm corresponding to scyllo-inositol and the triply serrated structure corresponding to taurine centered at 3.43 ppm do not appear on the total shape spectrum at $N_P = 54$. The two structures centered near 3.56 ppm and at 3.64 ppm corresponding to myoinositol are single peaks, whereas they should by triply serrated. The bottom panel of Fig. 8 shows the converged total absorption shape spectrum at $N_P = 800$ for the Padé-reconstructed prostate cancer data.

A comparison is given in Fig. 9 of the converged absorption component shape spectrum (top panel (i)) and total absorption shape spectrum (bottom panel (i)) for the Padé-reconstructed prostate cancer data. This is presented within the focused region from 2.40 to 3.70 ppm with $N_P = 800$. Once again, the triply and doubly serrated peaks seen on the total shape spectrum merely suggest the number of components, but it is only from the converged component spectrum reconstructed via the $\mathrm{FPT}^{(-)}$ that the true number of underlying resonances can be known unequivocally. As was seen for normal stromal prostate, the polyamine peaks are also small for malignant prostate and it would therefore be much more difficult than for the glandular case to determine from the total shape spectrum that there are exactly two PA components. Moreover, the citrate doublets centered near 2.53 and 2.73 ppm appear as broad peaks on the total shape spectrum and only a suggestion of doublet structures on the total

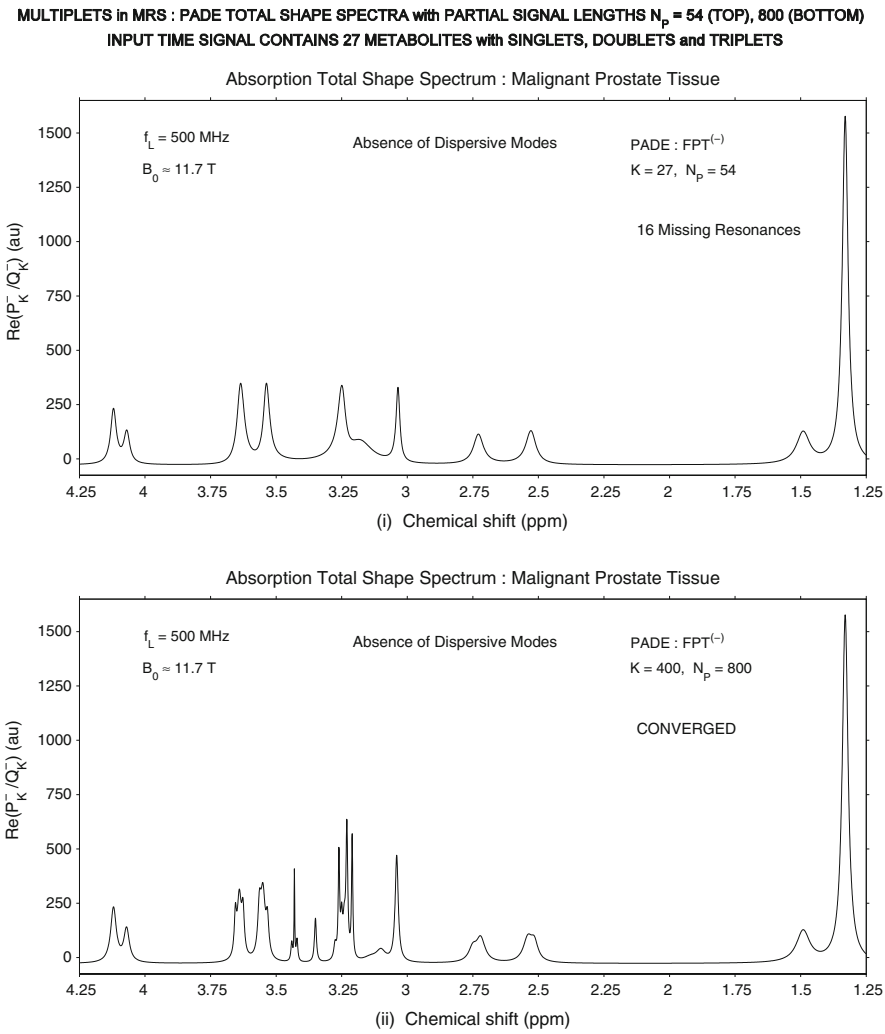

Fig. 8 Padé-reconstructed absorption total shape spectra for cancerous prostate, from in vitro data of Ref. [42]. The upper panel (i) is at $N_P = 54$ and the converged spectrum at $N_P = 800$ is shown in the bottom panel (ii)

shape spectrum. Both PC at 3.23 ppm and GPC at 3.24 ppm are completely resolved in the component shape spectrum, but not in the total shape spectrum which shows a single peak with a bulge to the left.

2.2.4 Comparison of the converged spectra for normal glandular prostate, normal stromal prostate and prostate cancer

In Figs. 10 and 11 the converged Padé-reconstructed absorption component and total shape spectra, respectively, are shown for the normal glandular prostate (top panels

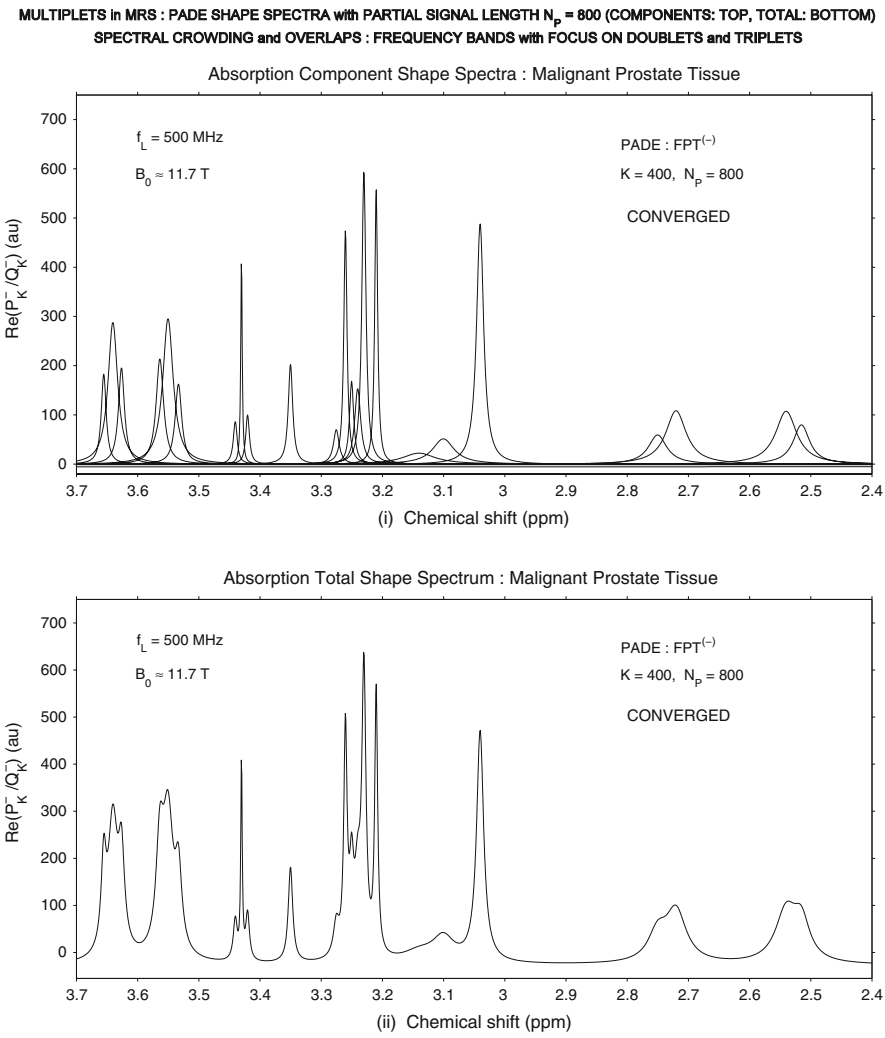

Fig. 9 Converged Padé-reconstructed absorption component shape spectra (top panel (i)) and converged absorption total shape spectra (bottom panel (ii)) for cancerous prostate, from in vitro data of Ref. [42]

(i)), normal stromal prostate (middle panel (ii)) and malignant prostate data (bottom panel (iii)). In the normal glandular prostate, after the lactate resonance at around 1.33 ppm, the most prominent spectral structures are the doublets of citrate doublets near 2.5 and 2.75 ppm, as well as the peaks corresponding to creatine around 3.04 ppm and the very narrow but tall resonance at around 3.21 ppm corresponding to choline. The two polyamine peaks are very broad and prominent, and there is a suggestion on the total shape spectrum that the leftward shoulder at around 3.14 ppm could possibly be a second component. As noted, this is clearly delineated on the component spectrum generated unequivocally, without fitting, via Padé-reconstruction.

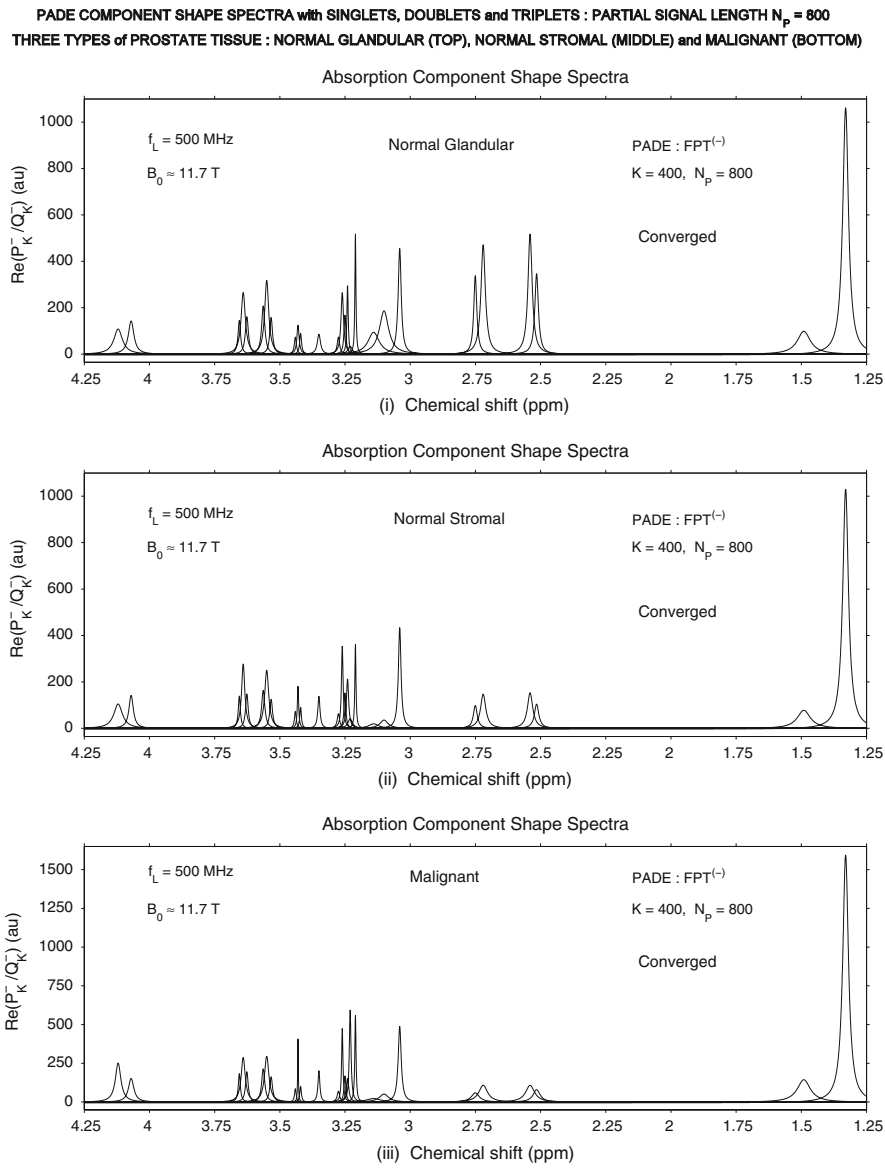

Fig. 10 Converged Padé-reconstructed absorption component spectra at $N_P = 800$, for normal glandular prostate (top panel (i)), normal stromal prostate (middle panel (ii)) and malignant prostate (bottom panel (iii)) derived from in vitro data of Ref. [42]

There are a number of distinctive features when examining the component and total absorption shape spectra of the normal stromal prostate as compared to those of the normal glandular tissue. Other than the lactate peaks near 1.33 and 4.12 ppm that are quite similar in these two cases, the intensity of the spectral structures is overall substantially lower for stromal tissue. The doublets of citrate doublets are markedly smaller, and the polyamines are just barely detectable for stromal tissue. The creatine

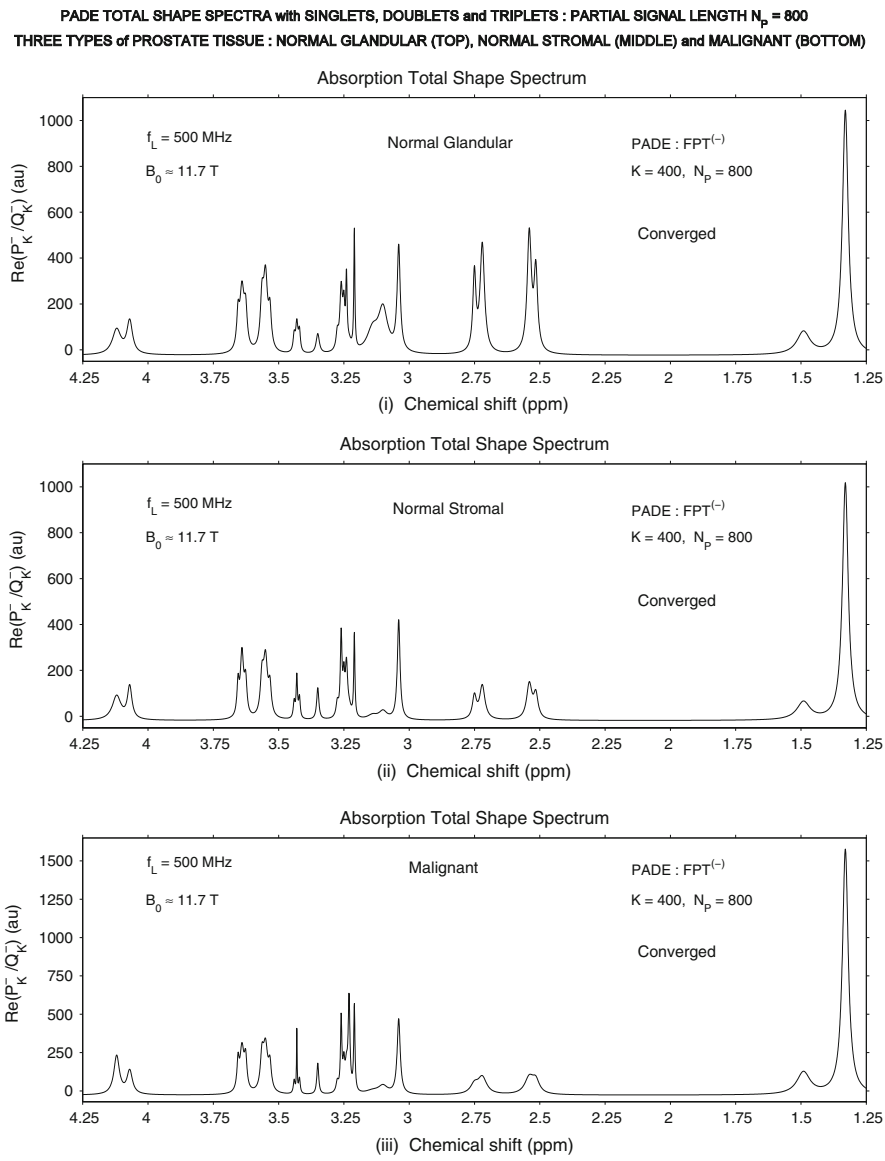

Fig. 11 Converged Padé-reconstructed absorption total shape spectra at $N_P = 800$, for normal glandular prostate (top panel (i)), normal stromal prostate (middle panel (ii)) and malignant prostate (bottom panel (iii)) derived from in vitro data of Ref. [42]

peak at 3.04 ppm is the most prominent after lactate at 1.33 ppm. The component spectrum is essential to visualize the two peaks centered at 3.10 and 3.14 ppm. The myoinositol triplet centered around 3.55 ppm is also notably smaller in the stromal prostate than in the normal glandular tissue.

The lactate peaks at 1.33 and 4.12 ppm in the malignant case are both larger than for the two normal tissues. The choline components at 3.21 to 3.24 ppm (i.e. total

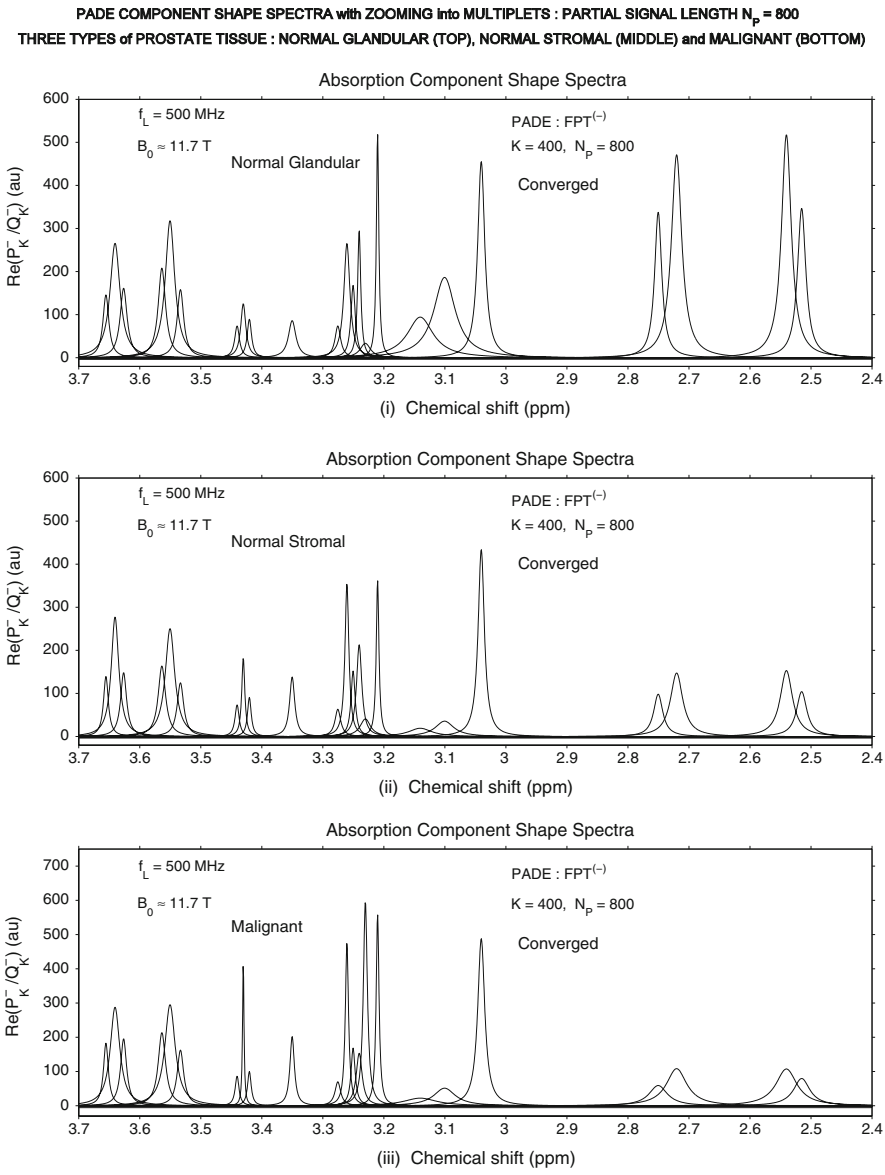

Fig. 12 Converged Padé-reconstructed absorption component spectra at $N_P = 800$, for normal glandular prostate (top panel (i)), normal stromal prostate (middle panel (ii)) and malignant prostate (bottom panel (iii)) within the zoomed region from 2.4 to 3.7 ppm derived from in vitro data of Ref. [42]

choline) are altogether more abundant than creatine at 3.04 ppm. The overall spectral pattern of the malignant case differs most clearly from normal glandular prostate. The spectrum for prostate cancer shows attenuation of the citrate doublet peaks and the two polyamine resonances, relative to the choline components.

In Figs. 12 and 13 we provide a comparison of the converged Padé-reconstructed absorption component and total shape spectra, respectively. Shown are the spectra for

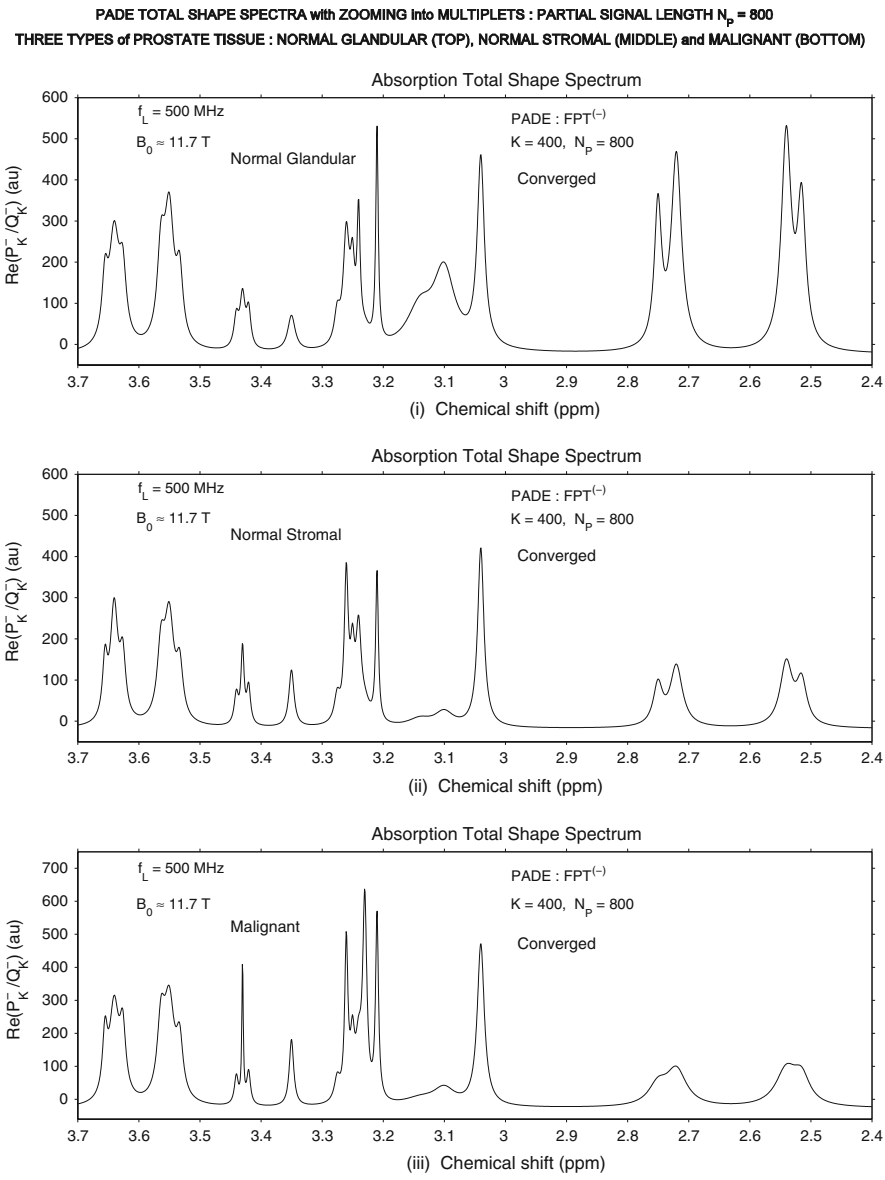

Fig. 13 Converged Padé-reconstructed absorption total shape spectra at $N_P = 800$, for normal glandular prostate (top panel (i)), normal stromal prostate (middle panel (ii)) and malignant prostate (bottom panel (iii)) within the zoomed region from 2.4 to 3.7 ppm derived from in vitro data of Ref. [42]

the normal glandular prostate (top panels (i)), normal stromal prostate (middle panel (ii)) and malignant prostate data (bottom panel (iii)) within the zoomed region from 2.40 to 3.70 ppm using the partial length $N_P = 800$. It is in this comparison that the component spectra are most elucidating, clearly delineating the PC and GPC peaks, which cannot be seen on the total shape spectrum.

3 Discussion

The present study demonstrates that the FPT can unequivocally resolve and exactly quantify multiplet resonances, including for regions of otherwise very high spectral density. As was seen by inspecting the total shape spectra alone, the actual number of resonances underlying a given peak, their positions and relative intensity can at best only be surmised by fitting, whose most abiding characteristic is non-uniqueness. It should be emphasized that using the residual spectrum as was done by Swanson et al. in Ref. [42] to indicate a good fit does not guarantee that the fit is the correct one. In our previous work, it was shown that convergence of the total shape spectrum does not necessarily imply that the component spectrum has done likewise [13,25]. Thus, the commonly employed practice of relying upon the residual spectrum to indicate convergence, is indeed tenuous, and, in fact, entails attempts to guess the number of resonances under a given peak, as customarily done by various post-processing fitting algorithms used in the MRS literature [43–45]. This is due to the reliance upon Fourier-based processing, which can only provide a total shape spectrum.

Using the FFT and fitting via the Levenberg-Marquardt algorithm, the authors of Ref. [42] acknowledge that spectral overlap directly impacted upon the accuracy of quantification. Moreover, procedures based upon integrating the areas under the peaks in the Fourier absorption spectra are vulnerable to subjectivity due to the uncertainty about lower and upper integration limits. Such techniques for reconstructing metabolite concentrations are recognized to be especially difficult with peak overlap [46].

In sharp contradistinction, Padé-based reconstruction in spectral analysis, because of its fundamental grounding in quantum mechanics and through the powerful concept of pole-zero cancellation (Froissart doublets), yields not only the possibility to exactly extract all the spectral frequencies and amplitudes of all the genuine resonances, but also provides certainty about their true number. The key clinical ramification of this latter feature is the unique, and, thus, the most reliable quantification of all the physical metabolite concentrations, including when there is an ample number of multiplet resonances, as seen in the present study. The "spectral crowding" problem does not obstruct the FPT, which via parametric analysis, without any fitting or numerical integration of peak areas, reconstructed all the multiplets and closely overlying resonances of different metabolites for all three problems under study, namely for normal glandular and normal stromal prostate, as well as for the spectra from prostate cancer.

Convergence was achieved for the normal glandular prostate data at a partial signal length $N_P = 700$ and for the normal stromal and the malignant data at $N_P = 600$ for the given total signal length $N = 1024$. At those partial signal lengths, the FPT exactly reconstructed all the spectral parameters for the time signals corresponding to the normal glandular and stromal prostate, and to the prostate cancer. Since $2K = N_P$, at the said convergence lengths N_P there was a total of 350, 300 and 300 resonances, respectively for the normal glandular prostate, normal stromal tissue and for the malignant case. Of these, only twenty-seven were true resonances, the other 323 and 273, respectively were spurious, and were identified as such by their zero amplitudes and the pole-zero coincidences. In other words, for these three tissues there were over eleven times and over ten times more spurious resonances than those that were genuine. It should be pointed out that the number of spurious resonances (and their percentage

in relation to those that are genuine) for the present prostate cancer MRS problem was much larger than for the ovarian cancer problem to which we applied the FPT [23,24], but fewer than for the breast cancer problem [25]. This reflects some of the more subtle features of spectral processing, particularly the density of the poles and zeros in the complex plane, the smallest distance among the poles and zeros, and inter-separations among poles and zeros [47].

In the present problems, it would be *theoretically* possible to retrieve all twenty-seven input resonances at $N_P = 54$ since there are 54 unknowns (27 complex frequencies and 27 complex amplitudes) with 54 linear equations and 54 signal points needed. In fact, at $N_P = 54$ twenty-seven resonances were retrieved. However, fifteen of these resonances were spurious for the normal glandular case and sixteen were spurious for the normal stromal and prostate cancer cases. These spurious resonances were identified by the pole-zero coincidences of the FPT (yielding zero-valued amplitudes), such that only the remaining twelve or eleven were genuine. Thus, via the powerful concept of Froissart doublets (pole-zero cancellations) the exact number of resonances is specified unequivocally. It is in this way that the FPT considers the true number of resonances as one of the unknown spectral quantities to be reconstructed, as opposed to the usual guessing in all fitting algorithms.

The process of convergence appears to begin at the outermost regions of the spectra, with lactate and alanine at about 1.33 and 1.49 ppm, respectively and with myoinositol and lactate at about 4.07 and 4.12 ppm, respectively. The inner, more congested spectral region converged subsequently. The last resonances to converge were those closest to the real axis with the smallest imaginary part of f_k. Notably, even at a few signal points prior to convergence, there can still be an admixture of the absorption and dispersive modes, since the latter appear intermittently. At convergence and beyond, the dispersive mode was completely absent, such that the final spectrum was purely in the absorption mode, i.e. the real part of the complex-valued spectrum. The stability of convergence was confirmed at longer partial signal lengths and at the total signal length for the three problems under present study and as has been the case in all our other applications of the FPT to MRS time signals [4,13,19,20,24,25,47].

It should also be noted that prior to but fairly near convergence, at $N_P = 600$ for the normal glandular data and at $N_P = 500$ for the normal stromal data, the phosphocholine resonance was still not identified and the calculated concentration of glycerophosphocholine was overestimated by even more than a missing PC concentration. For the malignant prostate data, even though phosphocholine was resolved prior to convergence, the concentration of GPC was still overestimated by about a factor of two (mention should also be made here concerning the ratio of GPC to PC, in relation to the so-called "glycerophosphocholine to phosphocholine switch" which appears to be an indicator of malignant transformation for e.g. breast [48]). However, all of the inaccuracies at an intermediate stage of calculation are gone upon reaching convergence, which occurs at $N_P = 700$ for the normal glandular prostate data and at $N_P = 600$ for normal stromal as well as for malignant prostate tissue. Viewed in this light, the capability of Padé-reconstruction to determine the exact number of genuine resonances and the precise point of convergence gains further relevance for improving cancer diagnostics through MRS.

As noted, the present problem was chosen because of its urgent clinical and public health importance. Namely, notwithstanding the striking success of MRS and MRSI in improving the accuracy with which prostatic tumor and extracapsular extension are detected, as well as helping to distinguish cancerous prostate from benign prostatic hypertrophy [36] and in aiding some aspects of therapeutic decision-making, there are still major challenges and difficulties for current applications of MRS within the area of prostate cancer. This should be seen in a broader framework; namely, that sensitive, specific, non-invasive methods for identifying prostate cancer are still beyond our reach.

On the basis of these input data from Ref. [42] for a limited number of prostate cancer samples, no definitive conclusions can be drawn about which metabolites are optimal for recognizing the presence of malignancy and distinguishing this from normal stromal and glandular tissue. Moreover, unfortunately, only the means and standard deviations of the calculated concentrations were given in Ref. [42] for the three types of tissue. Without data from the individual patients, or at least the minimum and maximum of the calculated concentrations, further inferences are tenuous. Nonetheless, there is still clearly a far richer source of spectral information with which to identify prostate cancer than is currently used with Fourier-based in vivo MRS. Padé-optimized MRS with its capacity to unequivocally resolve and quantify multiplet resonances and otherwise difficult spectra with numerous overlapping resonances could certainly contribute to further important insights.

The present study employs noise-free FIDs, since we wanted to set up the fully-controlled standard for the FPT in the case of the initial application of this method to data within the realm of prostate cancer diagnostics by MRS. As we have previously noted, this is methodologically justified [13,24,25]. We are now working to extend our analysis to both noise-corrupted synthesized data for the prostate (still well-controlled) and to encoded FIDs similar to those from Ref. [42] as well as in vivo MRS data from the prostate, and these results will be reported shortly in a follow-up study.

4 Conclusions

The fast Padé transform is shown to be optimally suited to unequivocally resolve and exactly quantify a large number of overlapping resonances, including multiplets of metabolites in one of the most challenging signal processing problems in MR spectroscopy. This is achieved using exclusively short time signals, and such an advantage is critical to encoded free induction decay data that become heavily corrupted with noise at the long total acquisition times required by the fast Fourier transform. Critically, we prove how the fast Padé transform can uniquely disentangle physical from spurious content of the studied time signals. The abundance of diagnostically important multiplets (notably doublet and triplet resonances) is characteristic of the spectra of healthy and cancerous prostate. We conclude that these advantages of the FPT could be of definite benefit for prostate cancer diagnostics via MRS. This line of investigation will continue with encoded data from normal, hypertrophic and cancerous tissue, in vitro and in vivo. We anticipate that Padé-optimized MRS will reduce the false positive rates of MR-based modalities and further improve their sensitivity. This could have

an important impact upon timely and accurate diagnosis of prostate cancer, as well as aiding decision-making for therapeutic dilemmas.

Acknowledgements This work has been supported by King Gustav the 5th Jubilee Foundation, the Signe and Olof Wallenius Stiftelse and the Karolinska Institute Research Fund.

References

1. A. Horwich, C. Parker, V. Kataja, ESMO Guidelines Working Group. Prostate cancer: ESMO clinical recommendations for diagnosis, treatment and follow-up. Ann. Oncol. **19**(Suppl 2), ii45 (2008)
2. V. Kundra, P.M. Silverman, S.F. Matin, H. Choi, Imaging in oncology from the University of Texas M. D. Anderson Cancer Center: diagnosis, staging, and surveillance of prostate cancer. Am. J. Roentgenol. **189**, 830 (2007)
3. H.L. Scher, in *Hyperplastic and Malignant Diseases of the Prostate*, ed. by E. Braunwald, A. Fauci, D.L. Kasper, S.L. Hauser, D.L. Longo, J.L. Jameson. Harrison's Principles of Internal Medicine, 15th edn. (McGraw-Hill, New York, 2001), pp. 608–616
4. Dž. Belkić, *Quantum Mechanical Signal Processing and Spectral Analysis* (Institute of Physics Publishing, Bristol, 2004)
5. P.A. Bottomley, The trouble with spectroscopy papers. J. Magn. Reson. Imaging **2**, 1 (1992)
6. Dž. Belkić, K. Belkić, Decisive role of mathematical methods in early cancer diagnostics. J. Math. Chem. **42**, 1–35 (2007)
7. Dž. Belkić, P.A. Dando, J. Main, H.S. Taylor, Three novel high-resolution nonlinear methods for fast signal processing. J. Chem. Phys. **113**, 6542 (2000)
8. Dž. Belkić, Fast Padé Transform (FPT) for magnetic resonance imaging and computerized tomography. Nucl. Instrum. Methods Phys. Res. A **471**, 165 (2001)
9. Dž. Belkić, Strikingly stable convergence of the fast Padé transform (FPT) for high-resolution parametric and non-parametric signal processing of Lorentzian and non-Lorentzian spectra. Nucl. Instrum. Methods Phys. Res. A **525**, 366 (2004)
10. Dž. Belkić, Error analysis through residual frequency spectra in the fast Padé transform (FPT). Nucl. Instrum. Methods Phys. Res. A **525**, 379 (2004)
11. Dž. Belkić, Analytical continuation by numerical means in spectral analysis using the fast Padé transform (FPT). Nucl. Instrum. Methods Phys. Res. A **525**, 372 (2004)
12. Dž. Belkić, K. Belkić, The fast Padé transform in magnetic resonance spectroscopy for potential improvements in early cancer diagnostics. Phys. Med. Biol. **50**, 4385 (2005)
13. Dž. Belkić, Exact quantification of time signals in Padé-based magnetic resonance spectroscopy. Phys. Med. Biol. **51**, 2633 (2006)
14. Dž. Belkić, Exponential convergence rate (the spectral convergence) of the fast Padé transform for exact quantification in magnetic resonance spectroscopy. Phys. Med. Biol. **51**, 6483 (2006)
15. Dž. Belkić, K. Belkić, The general concept of signal-noise separation (SNS): mathematical aspects and implementation in magnetic resonance spectroscopy. J. Math. Chem. (2008). doi:10.1007/s10910-007-9344-5
16. Dž. Belkić, K. Belkić, Unequivocal disentangling genuine from spurious information in time signals: Clinical relevance in cancer diagnostics through magnetic resonance spectroscopy. J. Math. Chem. (2008). doi:10.1007/s10910-007-9337-4
17. Dž. Belkić, K. Belkić, In vivo magnetic resonance spectroscopy by the fast Padé transform. Phys. Med. Biol. **51**, 1049 (2006)
18. M. Froissart, Approximation de Padé: Application à la Physique des Particules Élémentaires, CNRS, RCP, Programme No. 25. Strasburg **9**, 1 (1969)
19. Dž. Belkić, Machine accurate quantification in magnetic resonance spectroscopy. Nucl. Instrum. Methods Phys. Res. A **580**, 1034 (2007)
20. Dž. Belkić, Strikingly stable convergence of the fast Padé transform. J. Comp. Meth. Sci. Eng. **3**, 299 (2003)
21. Dž. Belkić, Padé-based magnetic resonance spectroscopy (MRS). J. Comp. Meth. Sci. Eng. **3**, 563 (2003)

22. W.W.F. Pijnappel, A. van den Boogaart, R. de Beer, D. van Ormondt, SVD-based quantification of magnetic resonance signals. J. Magn. Reson. **97**, 122 (1992)
23. K. Belkić, Resolution performance of the fast Padé transform: potential advantages for magnetic resonance spectroscopy in ovarian cancer diagnostics. Nucl. Instrum. Methods Phys. Res. A **580**, 874 (2007)
24. Dž. Belkić, K. Belkić, Mathematical modeling of an NMR chemistry problem in ovarian cancer diagnostics. J. Math. Chem. **43**, 395 (2008)
25. Dž. Belkić, K. Belkić, Exact quantification of time signals from magnetic resonance spectroscopy by the fast Padé transform with applications to breast cancer diagnostics. J. Math. Chem. doi:10.1007/s10910-008-9462-8
26. I.M. Thompson, D.K. Pauler, P.J. Goodman et al., Prevalence of prostate cancer among men with a prostate-specific antigen level $\leq$4.0 ng per milliliter. N. Engl. J. Med. **350**, 2239–2246 (2004)
27. L.S. Lim, K. Sherin, ACPM Prevention Practice Committee, Screening for prostate cancer in U.S. men: ACPM position statement on preventive practice. Am. J. Prev. Med. **34**, 164–170 (2008)
28. U.S. Preventive Services Task Force Screening for prostate cancer: U.S. Preventive Services Task Force Recommendation Statement. Ann. Intern. Med. **149**, 185–191 (2008)
29. K. Lin, R. Lipsitz, T. Miller, S. Janakiraman, U.S. Preventive Services Task Force Benefits and harms of prostate-specific antigen screening for prostate cancer: an evidence update for the U.S. Preventive Services Task Force. Ann. Intern. Med. **149**, 192–199 (2008)
30. D.K. Ornstein, J. Kang, How to improve prostate biopsy detection of prostate cancer. Curr. Urol. Rep. **2**, 218–223 (2001)
31. H. Hricak, MR imaging and MR spectroscopic imaging in the pre-treatment evaluation of prostate cancer. Br. J. Radiol. **78**, S103 (2005)
32. R. Huzjan, E. Sala, H. Hricak, Magnetic resonance imaging and magnetic resonance spectroscopic imaging of prostate cancer. Nat. Clin. Pract. Urol. **2**, 434 (2005)
33. L. Kwock, J.K. Smith, M. Castillo, M.G. Ewend, F. Collichio, D.E. Morris, T.W. Bouldin, S. Cush, Clinical role of proton magnetic resonance spectroscopy in oncology: brain, breast and prostate cancer. Lancet Oncol. **7**, 859 (2006)
34. S. Katz, M. Rosen, MR imaging and MR spectroscopy in prostate cancer management. Radiol. Clin. N. Am. **44**, 723 (2006)
35. R. Dhingsa, A. Qayyum, F.V. Coakley, Y. Lu, K.D. Jones, M.G. Swanson, P.R. Carroll, H. Hricak, J. Kurhanewicz, Prostate cancer localization with endorectal MR imaging and MR spectroscopic imaging: effect of clinical data on reader accuracy. Radiology **230**, 215 (2004)
36. J. Kuranewicz, M.G. Swanson, S.J. Nelson, D.B. Vigneron, Combined magnetic resonance imaging and spectroscopic imaging approach to molecular imaging of prostate cancer. J. Magn. Reson. Imaging **16**, 451–463 (2002)
37. K. Belkić, *Molecular Imaging through Magnetic Resonance for Clinical Oncology* (Cambridge International Science Publishing, Cambridge, UK, 2004)
38. M. Kaminogo, H. Ishimaru, M. Morikawa, M. Ochi, R. Ushijima, M. Tani, Y. Matsuo, J. Kawakubo, S. Shibata, Diagnostic potential of short echo time MR spectroscopy of gliomas with single-voxel and point-resolved spatially localised proton spectroscopy of brain. Neuroradiology **43**, 353 (2001)
39. J.M. Garcia-Segura, M. Sanchez-Chapado, C. Ibarburen, J. Viano, J.C. Angulo, J. Gonzalez, J.M. Rodriguez-Vallejo, In vivo proton magnetic resonance spectroscopy of disease prostate: spectroscopic features of malignant versus benign pathology. Magn. Reson. Imaging **17**, 755 (1999)
40. P. Swindle, S. McCredie, P. Russell, Pathologic characterization of human prostate tissue with proton MR spectroscopy. Radiology **228**, 144–151 (2003)
41. M.G. Swanson, D.B. Vigneron, Z.L. Tabatabai et al., Proton HR-MAS spectroscopy and quantitative pathologic analysis of MRI/3D-MRSI-targeted postsurgical prostate tissues. Magn. Reson. Med. **50**, 944 (2003)
42. M.G. Swanson, A.S. Zektzer, Z.L.Tabatabai, J. Simko, S. Jarso, K.R. Keshari, L. Schmitt, P.R. Carroll, K. Shinohara, D.B. Vigneron, J. Kurhanewicz, Quantitative analysis of prostate metabolites using 1H HR-MAS spectroscopy. Magn. Reson. Med. **55**, 1257 (2006)
43. J.W. van der Veen, R. de Beer, P.R. Luyten, D. van Ormondt, Accurate quantification of in vivo 31P NMR signals using the variable projection method and prior knowledge. Magn. Reson. Med. **6**, 92 (1988)
44. L. Vanhamme, A. van den Boogaart, S. van Haffel, Improved method for accurate and efficient quantification of MRS data with use of prior knowledge. J. Magn. Reson. **29**, 35–43 (1997)

45. S.W. Provencher, Estimation of metabolite concentrations from localized in vivo proton NMR spectra. Magn. Reson. Med. **30**, 672 (1993)
46. J. K. Nicholson, I.D. Wilson, High resolution proton magnetic resonance spectroscopy of biological fluids. Prog. NMR Spectrosc. **21**, 1245 (1989)
47. Dž. Belkić, Exact signal-noise separation by Froissart doublets in the Fast Padé transform for magnetic resonance spectroscopy. Adv Quantum Chem. 56 (2008, in press)
48. E.O. Aboagye, Z.M. Bhujwalla, Malignant transformation alters membrane choline phospholipid metabolism of human mammary epithelial cells. Cancer Res. **59**, 80 (1999)